

# Well-balanced high-order finite difference methods for systems of balance laws

Carlos Parés, Carlos Parés-Pulido  
University of Málaga (Spain), ETH Zürich (Switzerland)

July 18, 2022

## Abstract

In this paper, high order well-balanced finite difference weighted essentially non-oscillatory methods to solve general systems of balance laws are presented. Two different families are introduced: while the methods in the first one preserve every stationary solution, those in the second family only preserve a particular stationary solution. The accuracy, well-balancedness, and conservation properties of the methods are discussed, as well as their application to systems with singular source terms. The strategy is applied to derive third and fifth order well-balanced methods for a linear scalar balance law, Burgers' equation with a nonlinear source term, and for the shallow water model.

**Keywords:** Systems of balance laws, high-order methods, well-balanced methods, finite difference methods, weighted essentially non-oscillatory methods, Shallow Water model.

**Acknowledgments.** This research has been partially supported by the Spanish Government and FEDER through the Research project RTI2018-096064-B-C21.

## 1 Introduction

We consider 1d systems of balance laws of the form

$$U_t + F(U)_x = S(U)H_x, \quad (1)$$

where  $U(x, t)$  takes value in  $\Omega \subset \mathbb{R}^N$ ,  $F : \Omega \rightarrow \mathbb{R}^N$  is the flux function;  $S : \Omega \rightarrow \mathbb{R}^N$ ; and  $H$  is a known function from  $\mathbb{R} \rightarrow \mathbb{R}$  (possibly the identity function  $H(x) = x$ ). The system is supposed to be hyperbolic, i.e. the Jacobian  $J(U)$  of the flux function is assumed to have  $N$  different real eigenvalues. PDE systems of this form appear in many fluid models in different contexts: shallow water models, multiphase flow models, gas dynamic, elastic wave equations, etc.

Systems of the form (1) have non trivial stationary solutions that satisfy the ODE system:

$$F(U)_x = S(U)H_x. \quad (2)$$

The objective of well balanced schemes is to preserve exactly some of these steady state solutions. In the context of shallow water equations Bermúdez and Vázquez-Cendón introduced in [2] the condition called *C-property*: a scheme is said to satisfy this condition if it solves correctly the steady-state solutions corresponding to water at rest. Since then, the design of high-order well-balanced numerical methods for systems of balance laws has been a very active front of research: see, for instance, [1], [4], [5], [8], [9], [10], [11], [12], [13], [16] [17], [19], [22], [24], [28], [29], [30], [31], [34], [39] [40], [41], [42]...

We focus here on finite difference methods. Previous well-balanced high-order finite difference types have been based in techniques like the one proposed in [20] consisting on a formal transformation of (1) into a conservative system through the definition of a combined flux formed by the flux  $F$  and a primitive of the source term (see, for instance, [4], [16]). In [39]-[40], finite difference WENO schemes were applied to problems in which  $S(U)$  can be written as a function of variables that are constants for the stationary solutions to be preserved.

The technique introduced here is different and it is based on a simple idea: if  $U_i$  is the numerical approximation of the solution  $U(x_i, t)$  at the node  $x_i$  at time  $t$ , then if one can find a stationary solution  $U_i^*$  satisfying

$$U_i^*(x_i) = U_i,$$

one has

$$S(U_i)H_x(x_i) = S(U_i^*(x_i))H_x(x_i) = F(U_i^*(x_i))_x.$$

Therefore, the source term can be numerically computed with high order accuracy by applying the finite difference reconstruction operator to the point values  $\{F(U_i^*(x_j))\}$ . We will show that this simple strategy leads to high-order numerical methods that preserve either one particular stationary solution or all of them. Of course, the main difficulty comes from the computation of the stationary solution  $U_i^*$  at every node at every time step.

This strategy has been inspired by the concept of well-balanced reconstruction introduced in [5] to develop well-balanced high-order finite volume numerical methods: see [11] for a recent follow-up. In that case, a stationary solution whose average is the numerical approximation at every cell has to be computed at every time step. From this point of view, the technique introduced here for finite difference methods is easier, since the local problems to be solved are standard Cauchy problems for ODE system (2). In all the numerical tests considered here, explicit or implicit expressions of the stationary solutions are available, which will allow us to find  $U_i^*$  easily. For cases where this is not possible, a numerical method for ODE can be used to compute  $U_i^*$  at the stencil of  $x_i$  in the spirit of [6].

While the finite volume methods based on well-balanced reconstructions have the property of being conservative for any conservation law contained in (1) this is only the case for the finite difference methods that preserve one particular stationary solution to be described here but not for those that preserve every stationary solutions.

The case in which  $H$  has jump discontinuities will be also considered. At a discontinuity of  $H$ , a solution  $U$  is expected to be discontinuous too and the source term  $S(U)H_x$  cannot be defined within the distributional framework: it becomes a nonconservative product whose meaning has to be specified. There are different mathematical theories that allow one to give a sense to nonconservative products. In the theory developed in [15], nonconservative products are interpreted as Borel measures whose definition depends on the choice of a family of paths that, in principle, is arbitrary. As the Rankine-Hugoniot conditions, and thus the definition of weak solution, depend on the selected family of paths, its choice has to be consistent with the physics of the problem. Although for general nonconservative systems the adequate selection of paths may be difficult, in the case of systems of balance laws with singular source term there is a natural choice in which the paths are related to the stationary solutions of a regularized system: the interested reader is addressed to [11] for a detailed discussion. Although in general finite volume methods can be more easily adapted to deal with nonconservative products than finite difference schemes (see [32]), it will be shown that the numerical methods that preserve every stationary solution can be easily adapted to deal properly with singular source terms.

The organization of the article is as follows: finite difference high order methods based on a reconstruction operator are recalled in Section 2 where the particular example of WENO methods is highlighted. In Section 2 the case in which  $H$  is continuous and a.e. differentiable is considered. First, the numerical methods that preserve any stationary solution are introduced, together with the proofs of their accuracy and their well-balanced property. Next, methods that preserve only one stationary solution are introduced and the conservation property is discussed. The implementation of well-balanced WENO methods is also discussed. Section 3 is devoted to the more difficult case in which  $H$  is a.e. differentiable and piecewise continuous with isolated jump discontinuities. The definition of the nonconservative product is briefly discussed and the numerical methods introduced in Section 2 are adapted to this case. The numerical methods are applied to the linear transport equation with linear source term, Burgers' equation with a nonlinear source term, and the shallow water equations. In particular, it will be shown that the methods introduced here preserve all the stationary solutions for the shallow water, including cases in which the bottom has a step. Finally, some conclusions are drawn and further developments are discussed.

## 2 Numerical methods

### 2.1 General case

We will consider here high-order finite difference numerical methods for (1) based on a reconstruction operator, i.e. an operator which, given the point values of a function  $v(x)$  in the nodes of a mesh

$$v_i = v(x_i), \quad \forall i,$$

provides a numerical flux function

$$\hat{v}_{i+1/2} = \hat{v}(v_{i-r}, \dots, v_{i+s}), \quad \forall i,$$

such that the flux difference approximates the derivative  $v'(x)$  to  $k$ -th order accuracy

$$\frac{1}{\Delta x} (\hat{v}_{i+1/2} - \hat{v}_{i-1/2}) = v'(x_i) + O(\Delta x^k), \quad \forall i.$$

when  $v$  is smooth enough. Finite-difference ENO or WENO reconstructions are examples of such reconstruction operators: see [23], [35], [36]. Uniform meshes of constant step  $\Delta x$  will be considered and the following notation will be also used for the intercells

$$x_{i+1/2} = x_i + \frac{\Delta x}{2}.$$

Once the reconstruction operator has been chosen, a possible semi-discrete numerical method for solving (1) can be written as follows:

$$\frac{dU_i}{dt} + \frac{1}{\Delta x} (\hat{F}_{i+1/2} - \hat{F}_{i-1/2}) = S(U_i)H_x(x_i), \quad (3)$$

where  $\hat{F}_{i+1/2}$  are the flux reconstructions:

$$\hat{F}_{i+1/2} = \hat{F}(F(U_{i-r}), \dots, F(U_{i+s})), \quad (4)$$

The semidiscrete method (3) will be discretized in time by using TVD-RK methods: see [21].

### 2.2 WENO reconstructions

In the particular case of the WENO reconstruction of order  $p = 2k + 1$ , two flux reconstructions are computed using the values at the points  $x_{i-k}, \dots, x_{i+k}$ :

$$\hat{F}_{i+1/2}^L = \hat{F}^L(F(U_{i-k}), \dots, F(U_{i+k})), \quad (5)$$

$$\hat{F}_{i-1/2}^R = \hat{F}^R(F(U_{i-k}), \dots, F(U_{i+k})). \quad (6)$$

Once these reconstructions have been computed, an upwind criterion can be chosen to define  $\hat{F}_{i+1/2}$ . For instance, for scalar problems

$$u_t + f(u)_x = s(u)H_x, \quad (7)$$

an approximate value  $a_{i+1/2}$  of  $a(u) = f'(u)$  is chosen and the numerical flux is defined then as follows:

$$\hat{f}_{i+1/2} = a_{i+1/2}^+ f_{i+1/2}^L + a_{i+1/2}^- f_{i+1/2}^R,$$

where

$$a^\pm = \frac{1}{2}(a \pm |a|).$$

For systems, a matrix  $A_{i+1/2}$  with  $N$  real different eigenvalues

$$\lambda_{i+1/2,1}, \dots, \lambda_{i+1/2,N}$$

that approximates the Jacobian  $J(U)$  of the flux function has to be chosen and then the numerical flux can be defined by

$$\hat{F}_{i+1/2} = P_{i+1/2}^+ \hat{F}_{i+1/2}^L + P_{i+1/2}^- \hat{F}_{i+1/2}^R, \quad (8)$$

where

$$P_{i+1/2}^{\pm} = K_{i+1/2} D_{i+1/2}^{\pm} K_{i+1/2}^{-1}. \quad (9)$$

Here  $D_{i+1/2}^{\pm}$  is the diagonal matrix whose coefficients are

$$\frac{1}{2} (1 \pm \text{sign}(\lambda_{i+1/2,j})), \quad j = 1, \dots, N,$$

and  $K_{i+1/2}$  is a matrix whose columns are eigenvectors.

An alternative approach is to split the flux

$$F(U) = F^+(U) + F^-(U)$$

in such a way that the eigenvalues of the Jacobian  $J^+(U)$  (resp.  $J^-(U)$ ) of  $F^+(U)$  (resp.  $F^-(U)$ ) are positive (resp. negative). Then, the reconstruction operator is applied to  $F^{\pm}$ :

$$\widehat{F}_{i+1/2}^+ = \widehat{F}^L(F^+(U_{i-k}), \dots, F^+(U_{i+k})), \quad (10)$$

$$\widehat{F}_{i-1/2}^- = \widehat{F}^R(F^-(U_{i-k}), \dots, F^-(U_{i+k})), \quad (11)$$

and finally,

$$\widehat{F}_{i+1/2} = \widehat{F}_{i+1/2}^+ + \widehat{F}_{i+1/2}^-. \quad (12)$$

A standard choice is the Lax-Friedrichs flux-splitting:

$$F^{\pm}(U) = \frac{1}{2} (F(U) \pm \alpha U),$$

where  $\alpha$  is the maximum of the absolute value of the eigenvalues of  $\{J(U_i)\}$ , this maximum being taken over either local (WENO-LLF) or global (WENO-LF): see [23], [36].

In both cases (the upwind or the splitting implementations) the values used to compute  $\widehat{F}_{i+1/2}$  are those at the points

$$x_{i-k}, \dots, x_{i+k+1}$$

so that, in the general notation,  $r = k$  and  $s = k + 1$ .

### 3 Well-balanced high-order finite difference methods: $H$ continuous

#### 3.1 Definition of the method: general case

In order to tackle the difficulties gradually, let us suppose first that  $H$  is continuous and a.e. differentiable. In this case, the stationary solutions of (1) are the solutions of the ODE system:

$$\frac{d}{dx} F(U) = S(U) H_x. \quad (13)$$

Once the reconstruction operator has been chosen, the following semi-discrete numerical method is proposed:

$$\frac{dU_i}{dt} + \frac{1}{\Delta x} (\widehat{\mathcal{F}}_{i,i+1/2} - \widehat{\mathcal{F}}_{i,i-1/2}) = 0, \quad (14)$$

where  $\widehat{\mathcal{F}}_{i,i\pm 1/2}$  are computed as follows:

1. Look for the stationary solution  $U_i^*(x)$  such that:

$$U_i^*(x_i) = U_i. \quad (15)$$

2. Define

$$\mathcal{F}_j = F(U_j) - F(U_i^*(x_j)), \quad j = i - 1 - r, \dots, i + s$$

3. Compute

$$\begin{aligned}\widehat{\mathcal{F}}_{i,i+1/2} &= \widehat{\mathcal{F}}(\mathcal{F}_{i-r}, \dots, \mathcal{F}_{i+s}), \\ \widehat{\mathcal{F}}_{i,i-1/2} &= \widehat{\mathcal{F}}(\mathcal{F}_{i-1-r}, \dots, \mathcal{F}_{i-1+s}).\end{aligned}$$

The following result holds:

**Proposition 1.** *If the numerical method (3) is well-defined and the stationary solutions of (1) are smooth, then it has order of accuracy  $k$ .*

*Proof.* Let  $U(x, t)$  be a smooth solution of (1). Given a time  $t$  and an index  $i$ , the reconstruction procedure is applied to  $\{F(U(x_j, t) - F(U_i^{*,t}(x_j)))\}_{j=i-r}^{i+s+1}$  to obtain  $\widehat{\mathcal{F}}_{i,i\pm 1/2}$ , where  $U_i^{*,t}$  represents the solution of (17) that satisfies

$$U_i^{*,t}(x_i) = U(x_i, t). \quad (16)$$

One has:

$$\begin{aligned}\partial_t U(x_i, t) + \frac{1}{\Delta x} (\widehat{\mathcal{F}}_{i,i+1/2} - \widehat{\mathcal{F}}_{i,i-1/2}) \\ &= \partial_t U(x_i, t) + \partial_x F(U)(x_i, t) - \partial_x F(U_i^{*,t})(x_i) + O(\Delta x^k) \\ &= \partial_t U(x_i, t) + \partial_x F(U)(x_i, t) - S(U_i^{*,t}(x_i)) \partial_x H(x_i) + O(\Delta x^k) \\ &= \partial_t U(x_i, t) + \partial_x F(U)(x_i, t) - S(U(x_i, t)) \partial_x H(x_i) + O(\Delta x^k) \\ &= O(\Delta x^k),\end{aligned}$$

where the facts that  $U$  is a solution of (1) and  $U_i^{*,t}$  a stationary solution satisfying (16) have been used.  $\square$

Observe that the method is well-defined if the first step of the reconstruction procedure can be always performed, i.e. if for every  $i$  the Cauchy problem

$$\begin{cases} \frac{d}{dx} F(U) = S(U) H_x, \\ U(x_i) = U_i, \end{cases} \quad (17)$$

has a unique solution whose interval of definition contains the stencil  $x_{i-r}, \dots, x_{i+s+1}$ . When (17) has no solution, or when it has a unique one but the stencil is not contained in its interval of definition, the cell values  $\{U_i\}$ , to which the reconstruction operator is applied, cannot be the point values of a stationary solution of (1). In this case, there is no stationary solution to preserve and the numerical method (3) is applied to compute  $U_i$ . When (17) has more than one solution, an additional criterion is needed to select one of them in the first stage of the reconstruction procedure.

**Remark 1.** *In the notation  $\widehat{\mathcal{F}}_{i,i+1/2}$  the index  $i+1/2$  corresponds to the intercell and the index  $i$  to the center of the cell where the initial condition of (17) is imposed. Therefore, in general*

$$\widehat{\mathcal{F}}_{i,i+1/2} \neq \widehat{\mathcal{F}}_{i+1,i+1/2} \quad (18)$$

*as one can expect due to the non conservative nature of the system of equations. Notice that two reconstructions have to be computed at every stencil:  $\widehat{\mathcal{F}}_{i,i+1/2}$  and  $\widehat{\mathcal{F}}_{i+1,i+1/2}$ .*

**Remark 2.** *If the Jacobian  $J(U)$  of the flux function  $F(U)$  is regular, the ODE system can be written in normal form:*

$$\begin{cases} \frac{dU}{dx} = J(U)^{-1} S(U) H_x, \\ U(x_i) = U_i, \end{cases} \quad (19)$$

*and it is expected to have a unique maximal solution  $U_i^*$ . If one of the eigenvalues of  $J(U)$  vanishes in the stencil (the problem is said to be resonant in this case), (17) may have no solution or have more than one.*

### 3.2 Well-balanced property

The numerical method (14) is well-balanced in the sense given by the following

**Proposition 2.** *Given a stationary solution  $U^*$  of (1), the vector of its point values  $\{U^*(x_i)\}$  is an equilibrium of the ODE system given by the semi-discrete method (14).*

*Proof.* Observe that, in this case

$$U_i^{*,t} \equiv U^*, \quad \forall i, t$$

and thus

$$F(U^*(x_j)) - F(U_i^{*,t}(x_j)) = 0, \quad \forall i, j = i-1-r, \dots, i+s.$$

The proof is trivial from this equality.  $\square$

### 3.3 Numerical method with WENO reconstructions

Let us discuss the implementation of the numerical method (14) in the particular case of WENO reconstructions with the upwind or the flux-splitting approach.

#### 3.3.1 Upwind approach

The implementation in this case is as follows: once the solution  $U_i^*$  has been computed:

- Define

$$\mathcal{F}_j = F(U_j) - F(U_i^*(x_j)), \quad j = i-k-1, \dots, i+k+1$$

- Compute

$$\begin{aligned} \hat{\mathcal{F}}_{i,i+1/2}^L &= \hat{\mathcal{F}}^L(\mathcal{F}_{i-k}, \dots, \mathcal{F}_{i+k}), \\ \hat{\mathcal{F}}_{i,i-1/2}^R &= \hat{\mathcal{F}}^R(\mathcal{F}_{i-k}, \dots, \mathcal{F}_{i+k}), \\ \hat{\mathcal{F}}_{i,i+1/2}^R &= \hat{\mathcal{F}}^R(\mathcal{F}_{i-k+1}, \dots, \mathcal{F}_{i+k+1}), \\ \hat{\mathcal{F}}_{i,i-1/2}^L &= \hat{\mathcal{F}}^L(\mathcal{F}_{i-k-1}, \dots, \mathcal{F}_{i+k-1}). \end{aligned}$$

- Choose intermediate matrices  $A_{i\pm 1/2}$ .

- Define

$$\begin{aligned} \hat{\mathcal{F}}_{i,i+1/2} &= P_{i+1/2}^+ \hat{\mathcal{F}}_{i,i+1/2}^L + P_{i+1/2}^- \hat{\mathcal{F}}_{i,i+1/2}^R, \\ \hat{\mathcal{F}}_{i,i-1/2} &= P_{i-1/2}^+ \hat{\mathcal{F}}_{i,i-1/2}^L + P_{i-1/2}^- \hat{\mathcal{F}}_{i,i-1/2}^R, \end{aligned}$$

where the projection matrices  $P_{i\pm 1/2}^\pm$  are given by (9).

#### 3.3.2 Flux-splitting approach

The implementation of WENO with splitting approach will be as follows: once the solution  $U_i^*$  has been computed:

- Define

$$\begin{aligned} \mathcal{F}_j^+ &= F^+(U_j) - F^+(U_i^*(x_j)), \quad j = i-k-1, \dots, i+k \\ \mathcal{F}_j^- &= F^-(U_j) - F^-(U_i^*(x_j)), \quad j = i-k, \dots, i+k+1 \end{aligned}$$

- Compute

$$\begin{aligned}
\widehat{\mathcal{F}}_{i,i+1/2}^+ &= \widehat{\mathcal{F}}^+{}^L(\mathcal{F}_{i-k}^+, \dots, \mathcal{F}_{i+k}^+), \\
\widehat{\mathcal{F}}_{i,i-1/2}^- &= \widehat{\mathcal{F}}^-{}^R(\mathcal{F}_{i-k}^-, \dots, \mathcal{F}_{i+k}^-), \\
\widehat{\mathcal{F}}_{i,i+1/2}^- &= \widehat{\mathcal{F}}^-{}^R(\mathcal{F}_{i-k+1}^-, \dots, \mathcal{F}_{i+k+1}^-), \\
\widehat{\mathcal{F}}_{i,i-1/2}^+ &= \widehat{\mathcal{F}}^+{}^L(\mathcal{F}_{i-k-1}^+, \dots, \mathcal{F}_{i+k-1}^+).
\end{aligned}$$

- Define

$$\widehat{\mathcal{F}}_{i,i\pm 1/2} = \widehat{\mathcal{F}}_{i,i\pm 1/2}^- + \widehat{\mathcal{F}}_{i,i\pm 1/2}^+.$$

In the particular case of the Lax-Friedrichs splitting, the reconstruction operators  $\mathcal{F}^L$  and  $\mathcal{F}^R$  will be applied to the values

$$F(U_j) - F(U_i^*(x_j)) \pm \alpha(U_j - U_i^*(x_j))$$

in the corresponding stencil. Again  $\alpha$  is the local or global maximum eigenvalue of  $\{J(U_i)\}$ : although  $U_i^*$  is not explicitly taken into account in the numerical viscosity, the numerical method has been shown to be stable under a CFL number of 1/2 in all the test cases considered here.

**Remark 3.** Observe that, while for a conservative system 2 reconstructions are computed at every stencil  $x_{i-k}, \dots, x_{i+k}$ , 4 reconstructions have to be computed at every stencil: 2 using  $U_i^*$ , 1 using  $U_{i-1}^*$ , 1 using  $U_{i+1}^*$ .

### 3.4 Numerical methods that preserve only one stationary solution

If there is only one known stationary solution  $U^*(x)$  to preserve (which is the case if, for instance, the initial condition is a perturbation of a given steady state), the following semidiscrete numerical method can be used:

$$\frac{dU_i}{dt} + \frac{1}{\Delta x} (\widehat{\mathcal{F}}_{i+1/2} - \widehat{\mathcal{F}}_{i-1/2}) = (S(U_i) - S(U^*(x_i)))H_x(x_i), \quad (20)$$

where  $\widehat{\mathcal{F}}_{i\pm 1/2}$  are computed now as follows:

1. Apply the reconstruction operator to the point values

$$\mathcal{F}_j = F(U_j) - F(U^*(x_j)), \quad j = i - r, \dots, i + s$$

to obtain

$$\widehat{\mathcal{F}}_{i+1/2} = \widehat{\mathcal{F}}(\mathcal{F}_{i-r}, \dots, \mathcal{F}_{i+s}).$$

2. Apply the reconstruction operator to the point values

$$\mathcal{F}_j = F(U_j) - F(U^*(x_j)), \quad j = i - 1 - r, \dots, i - 1 + s$$

to obtain

$$\widehat{\mathcal{F}}_{i-1/2} = \widehat{\mathcal{F}}(\mathcal{F}_{i-r}, \dots, \mathcal{F}_{i+s}).$$

It can be easily checked that this method preserves the stationary solution  $U^*$  and, if this solution is smooth enough, the order of the method is equal to that of the reconstruction operator. Observe that the first stage of the reconstruction procedure, that consisted of the resolution of a Cauchy problem for a ODE system, is avoided; therefore the computational cost is expected to be lower than that of the methods that preserve any stationary solution.

Another important difference between numerical methods (14) and (20) lies in their conservation properties: let us assume that there exists  $I \in \{1, \dots, N\}$  such that:

$$S(U) = [0, \dots, 0, S_{I+1}(U), \dots, S_N(U)]^T,$$

i.e. the first  $I$  equations of (1) are conservation laws. Then, (20) is conservative for these equations: in effect, the first  $I$  components reduce to the conservative expressions:

$$\frac{du_{j,i}}{dt} + \frac{1}{\Delta x} \left( \widehat{f}_{j,i+1/2} - \widehat{f}_{j,i-1/2} \right) = 0, \quad j = 1, \dots, I,$$

where  $u_{j,i}$  and  $\widehat{f}_{j,i+1/2}$  represent respectively the  $j$ th component of  $U_i$  and  $\widehat{\mathcal{F}}_{i+1/2}$ . This is not the case for (14) since inequality (18) is expected to hold at every component for (14) due to the fact that, in general,  $U_i^* \neq U_{i+1}^*$ .

## 4 Well-balanced high-order finite difference methods: $H$ discontinuous

Let us suppose now that  $H$  is a.e. differentiable with finitely many isolated jump discontinuities. In this case, the definition of weak solutions (and, in particular, of stationary solutions) of (1) becomes more difficult: a solution  $U$  is expected to be discontinuous at the discontinuities of  $H$  and, in this case, the source term  $S(U)H_x$  cannot be defined within the distributional framework. The source term becomes then a nonconservative product that can be defined in infinitely many different forms: see [15]. Like in [11], the following criterion is assumed here to define the weak solutions of (1):

(AC) A pair of states  $(U^-, U^+)$  can be the limits of an admissible weak solution of (1) to the left and to the right of a discontinuity point of  $H$ ,  $x^*$ , if and only if there exists a solution of the ODE system

$$\frac{d}{d\sigma} F(V) = S(V) \tag{21}$$

satisfying

$$V(H^\pm) = U^\pm. \tag{22}$$

This admissibility criterion can be understood as a particular choice of paths within the theory developed by DalMasso, LeFloch, and Murat in [15] that allows one to give a sense to the nonconservative product as a Borel measure. In [11] it has been shown that the admissible jumps according to this criterion can be regularized through a smooth stationary solution in the following sense:  $(U^-, U^+)$  is an admissible jump at a discontinuity point  $x^*$  of  $H$  if and only if for any given  $\epsilon > 0$  it is possible to find two smooth functions  $U_\epsilon$ ,  $H_\epsilon$  defined in  $(x^* - \epsilon, x^* + \epsilon)$  such that  $H_\epsilon$  is monotone and:

$$\begin{aligned} \lim_{x \rightarrow x^* - \epsilon} U_\epsilon(x) &= U^-, & \lim_{x \rightarrow x^* + \epsilon} U_\epsilon(x) &= U^+, \\ \lim_{x \rightarrow x^* - \epsilon} H_\epsilon(x) &= H(x^{*-}), & \lim_{x \rightarrow x^* + \epsilon} H_\epsilon(x) &= H(x^{*+}), \\ \partial_x F(U_\epsilon) &= S(U_\epsilon) \partial_x H_\epsilon, & \text{in } (x^* - \epsilon, x^* + \epsilon). \end{aligned}$$

Moreover, the jumps at the discontinuities of  $H$  can be interpreted as stationary contact discontinuities of an extended system and the admissibility criterion (AC) is equivalent to assuming that Riemann invariants are preserved through these discontinuities (see [11] for details).

Let us remark that, if  $V(\sigma)$  is a solution of (21), then  $U(x) = V(H(x))$  is a stationary solution of (1): observe that (13) is trivially satisfied in smooth regions and (AC) is trivially satisfied in discontinuities. The well-balanced numerical method (14) can be easily adapted to this case by looking for stationary solutions of this form. More precisely, let us assume that the mesh has been designed so that the discontinuities of  $H$  lie in intercells. Then, the numerical method (14) can be still applied with the only difference that now the first stage of the reconstruction step (15) is now as follows:

1. Look for the solution  $V_i^*(\sigma)$  of (21) such that:

$$V_i^*(H_i) = U_i, \tag{23}$$

where  $H_i = H(x_i)$ .



Every discontinuity point  $x^*$  will be placed at an intercell  $x_{I-1/2}$ . The reconstruction so defined leads to the following approximation of the Dirac delta produced by the discontinuity of  $H$ :

$$(F(V(H^+(x_{I-1/2}))) - F(V(H^-(x_{I-1/2})))) \delta|_{x=x^*}, \quad (24)$$

where  $V(\sigma)$  is a solution of (21): therefore, it is consistent with the assumed definition of the nonconservative products. Although consistency is not enough to guarantee the convergence to the right weak solution of nonconservative systems (see [33], [7]) the numerical tests in Section 5 show that the numerical methods capture the correct weak solutions.

In order to compare the behaviour of the different methods in the presence of a discontinuity of  $H$ , for WENO methods (1) the Dirac delta issued from a discontinuity of  $H$  will be approached by

$$S_{I-1/2} \frac{H^+(x_{I-1/2}) - H^-(x_{I-1/2})}{\Delta x} \delta|_{x=x^*}, \quad (25)$$

where  $S_{I-1/2}$  is some intermediate value of  $S(U)$  at the discontinuity. An upwind treatment of the singular source term is then used, so that the numerical method for the neighbor nodes writes as follows:

$$\begin{aligned} \frac{dU_{I-1}}{dt} + \frac{1}{\Delta x} (\hat{F}_{I-1/2} - \hat{F}_{I-3/2}) &= S(U_{I-1})H_x(x_{I-1}) + S_{I-1/2}^-, \\ \frac{dU_I}{dt} + \frac{1}{\Delta x} (\hat{F}_{I+1/2} - \hat{F}_{I-1/2}) &= S(U_I)H_x(x_I) + S_{I-1/2}^+, \end{aligned} \quad (26)$$

where

$$S_{I-1/2}^\pm = P_{i+1/2}^\pm S_{I-1/2} \frac{H(x_I) - H(x_{I-1})}{\Delta x}.$$

Here,  $P_{i+1/2}^\pm$  are the projection matrices given by (9). It will be seen in Section 5 that these methods do not converge to the assumed weak solutions. Moreover, the behaviour of the numerical methods at the discontinuity of  $H$  depends both on  $\Delta x$  and the chosen intermediate state.

In the case of the methods that only preserve one stationary solution  $U^*$ , the source term in the neighbor nodes of the discontinuity will be computed as follows:

$$\begin{aligned} \frac{dU_{I-1}}{dt} + \frac{1}{\Delta x} (\hat{\mathcal{F}}_{I-1/2} - \hat{\mathcal{F}}_{I-3/2}) &= (S(U_{I-1}) - S(U^*(x_{I-1})))H_x(x_{I-1}) + S_{I-1/2}^- - S_{I-1/2}^{*-}, \\ \frac{dU_I}{dt} + \frac{1}{\Delta x} (\hat{\mathcal{F}}_{I+1/2} - \hat{\mathcal{F}}_{I-1/2}) &= (S(U_I) - S(U^*(x_I)))H_x(x_I) + S_{I-1/2}^+ - S_{I-1/2}^{*+}, \end{aligned} \quad (27)$$

with

$$S_{I-1/2}^{*\pm} = P_{i+1/2}^\pm S_{I-1/2}^* \frac{H(x_I) - H(x_{I-1})}{\Delta x}.$$

Clearly, if  $U_i = U^*(x_i)$  for  $i = I-1, I$  the right-hand sides vanish and the approximation of the Dirac mass is given again by (24) but, if it is not the case, a combination of (24) and (25) is used. Therefore, this method is only consistent with the definition of weak solution when the stationary solution  $U^*$  is not perturbed at the neighbour nodes of the discontinuity, as it will be seen in Section 5

## 5 Numerical tests

In this section we apply the numerical methods introduced in Sections 2 and 3 to a number of test cases with  $H$  continuous or discontinuous. Three families of methods based on WENO reconstructions of order  $p$  will be compared:

- WENO $p$ : methods of the form (3).
- WBWENO $p$ : methods of the form (14) that preserve any stationary state.
- WB1WENO $p$ : methods of the form (20) that preserve only one given stationary state.

Nevertheless, in many test cases the results obtained with WBWENO $p$  and WB1WENO $p$  are indistinguishable: in those cases, only the results corresponding to WBWENO $p$  will be shown. In all cases, the global Lax-Friedrichs flux-splitting approach is used for WENO implementation and the third order TVD-RK3 method is applied for the time discretization: see [21]. The CFL parameter is set to 0.5.

## 5.1 A linear problem

We consider the linear scalar problem

$$u_t + u_x = uH_x. \quad (28)$$

In this case, (21) reduces to

$$\frac{dv}{d\sigma} = v, \quad (29)$$

whose solutions are

$$V(\sigma) = Ce^\sigma, \quad C \in \mathbb{R}.$$

The stationary solutions of (28) for any given  $H$  are thus given by:

$$u^*(x) = Ce^{H(x)}, \quad C \in \mathbb{R}. \quad (30)$$

The solution of (23) is thus

$$v_i^*(\sigma) = u_i e^{\sigma - H_i}.$$

Therefore, well-balanced methods are based on the reconstructions of

$$f_j = u_j - u_i e^{(H_j - H_i)\Delta x}, \quad j = i - r, \dots, i + s.$$

### 5.1.1 Order test

Let us consider (28) with

$$H(x) = x.$$

It can be easily checked that the solution of (28) with initial condition:

$$u(x, 0) = u_0(x), \quad x \in \mathbb{R}$$

is given by

$$u(x, t) = e^t u_0(x - t), \quad x \in \mathbb{R}.$$

Let us consider the initial condition:

$$u_0(x) = \begin{cases} 0 & \text{if } x < 0, \\ p(x) & \text{if } 0 \leq x \leq 1, \\ 1 & \text{otherwise,} \end{cases} \quad (31)$$

where  $p$  is the 11th degree polynomial

$$p(x) = x^6 \left( \sum_{k=0}^5 (-1)^k \binom{5+k}{k} (1-x)^k \right)$$

such that

$$p(0) = 0, \quad p(1) = 1, \quad p^k(0) = p^k(1) = 0, \quad k = 1, \dots, 5$$

see Figure 1.

We solve (28) with initial condition (31) with well-balanced and non well-balanced third order methods in the interval  $[-2, 10]$ . Free boundary conditions based on the use of ghost cells are used at both extremes. Table 1 shows the  $L^1$ -errors and the empirical order of convergence corresponding to WENO $p$  and WBWENO $p$ ,  $p = 3, 5$ . As can be seen, both methods are of the expected order and the errors corresponding to methods of the same order are almost identical. In order to capture the expected order, the smooth indicators of the WENO reconstruction have been set to 0 and  $\Delta t = \Delta x^{5/3}$  has been chosen for the fifth order methods.

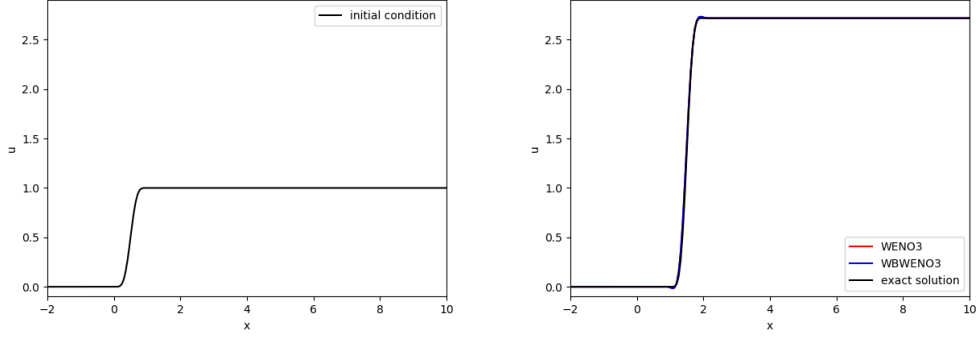


Figure 1: Test 5.1.1: initial condition (left). Exact solution and numerical solution obtained with WBWENO3 and WBWENO5 at time  $t = 1$  using a mesh of 200 cells

Cells	WENO3		WBWENO3		WENO5		WBWENO5	
	Error	Order	Error	Order	Error	Order	Error	Order
100	1.000E-1	-	1.023E-1	-	4.0902E-2	-	4.0910E-2	-
200	2.053E-2	2.28	2.084E-2	2.29	2.4404E-3	4.06	2.4407E-3	4.06
400	2.978E-3	2.78	3.019E-3	2.78	9.1307E-5	4.74	9.1315E-5	4.74
800	3.815E-4	2.96	3.867E-4	2.96	3.0118E-6	4.92	3.0121E-6	4.92
1600	4.788E-5	2.99	4.855E-5	2.99	9.4849E-8	4.98	9.4857E-8	4.98

Table 1: Test 5.1.1. Errors in  $L^1$  norm and convergence rates for WB $p$  and WBWENO $p$ ,  $p = 3, 5$  at time  $t = 1$ .

### 5.1.2 A moving discontinuity linking two stationary solutions

Next, we consider (28) with again  $H(x) = x$ , and initial condition

$$u_0(x) = \begin{cases} 4e^x & \text{if } x < 0, \\ e^x & \text{otherwise.} \end{cases}$$

The solution consists of a discontinuity linking two steady states that travels at speed 1:

$$u(x, t) = \begin{cases} 4e^x & \text{if } x < t, \\ e^x & \text{otherwise.} \end{cases}$$

Figure 2 shows the exact and the numerical solutions at time  $t = 1$  obtained with WBWENO3 and WENO3 (left) and a zoom of the differences of the numerical and the exact solution at the same time (right). It can be observed that the stationary states at both sides of the discontinuity are better captured with the well-balanced method. For fifth order methods the differences are lower, but still noticeable: see Figure 3. The results obtained with WBWENO $p$ , and the WB1WENO $p$ ,  $p = 3, 5$  that only preserve the stationary solution  $u^*(x) = 4e^x$ , are indistinguishable.

## 5.2 Burgers' equation with source term

We consider next the scalar equation

$$u_t + f(u)_x = s(u)H_x, \quad (32)$$

with

$$f(u) = \frac{1}{2}u^2, \quad s(u) = u^2.$$

The stationary solutions are also given by (30). The reconstruction operator has to be applied in this case to

$$f_j = \frac{u_j^2}{2} - \frac{u_i^2 e^{2(H_j - H_i)\Delta x}}{2}, \quad j = i - r, \dots, i + s.$$

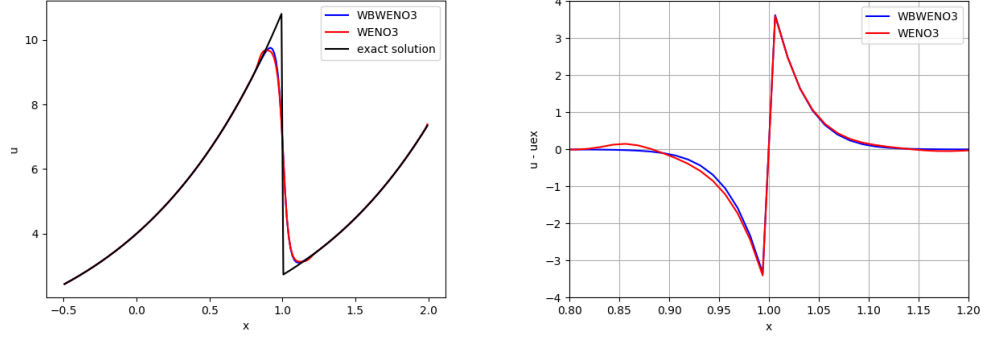


Figure 2: Test 5.1.2: exact solution and numerical solutions obtained with WBWENO3 and WENO3 using a mesh of 200 cells,  $t = 1$  (left); zoom of the differences between the numerical and the exact solutions (right)

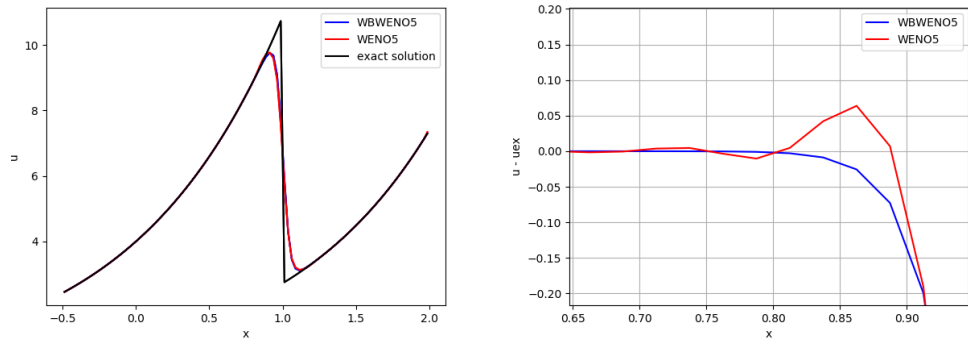


Figure 3: Test 5.1.2: exact solution and numerical solutions obtained with WBWENO5 and WENO5 using a mesh of 100 cells,  $t = 1$  (left); zoom of the differences between the numerical and the exact solutions (right)

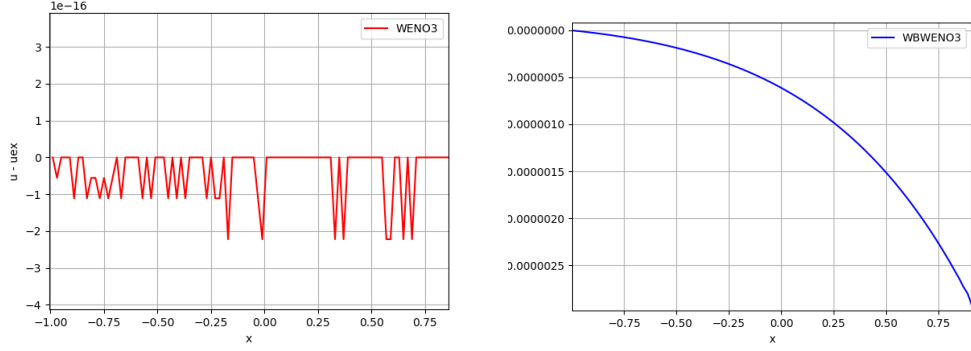


Figure 4: Test 5.2.1: zoom of the differences between the numerical solutions at time  $t = 8$  and the stationary solution using a 200-cell mesh. Left: WBWENO3. Right: WENO3

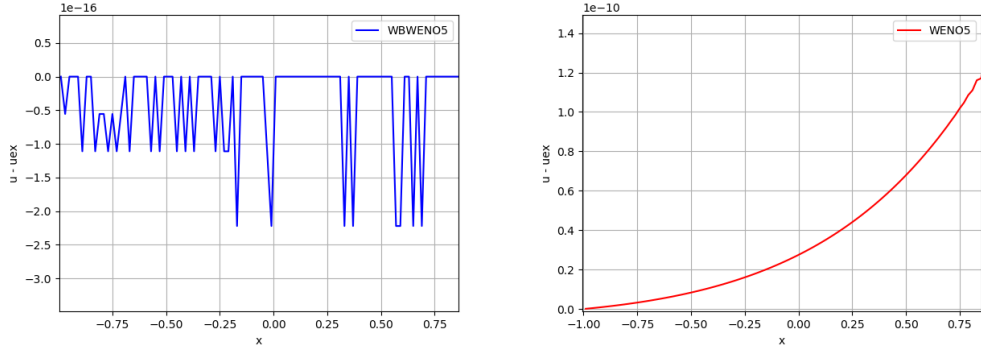


Figure 5: Test 5.2.1: zoom of the differences between the numerical solutions at time  $t = 8$  and the stationary solution using a 200-cell mesh. Left: WBWENO5. Right: WENO5

### 5.2.1 Preservation of a stationary solution with smooth $H$

In this test case we consider  $H(x) = x$  and the stationary solution

$$u(x) = e^x. \quad (33)$$

Let us solve (32) taking this stationary solution as initial condition in the interval  $[-1, 1]$ . As boundary conditions, the value of the stationary solution is imposed at the ghost cells. Figures 4 and 5 show the differences between the stationary solution and the numerical solutions obtained at time  $t = 8$  with WENO $p$  and WBWENO $p$ ,  $p = 3, 5$  using a 200-cell mesh: the well-balanced methods capture the stationary solution with machine accuracy. This is confirmed by Tables 2 and 3 that show the  $L^1$ -errors and the empirical order of convergence corresponding to WENO $p$  and WBWENO $p$ ,  $p = 3, 5$ .

Cells	WENO3		WBWENO3
	Error	Order	Error
100	1.9044E-06	-	8.9928E-17
200	2.4762E-07	2.94	1.4543E-16
400	3.1550E-08	2.97	1.5304E-14
800	3.9817E-09	2.98	1.6560E-14

Table 2: Test 5.2.1. Errors in  $L^1$  norm and convergence rates for WB3 and WBWENO3 at time  $t = 8$ .

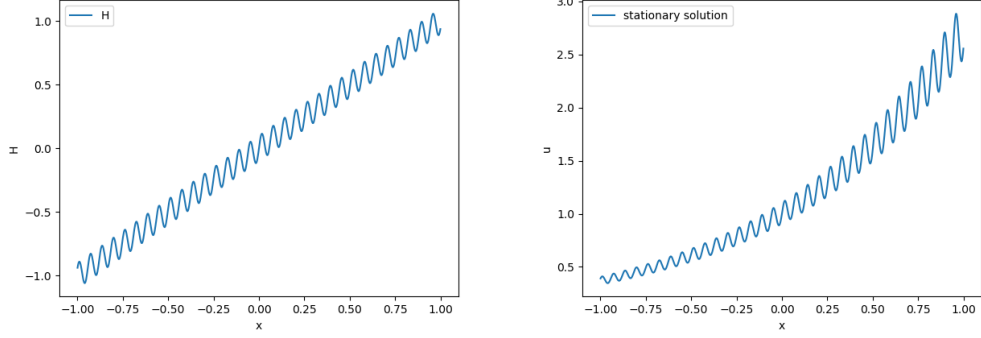


Figure 6: Test 5.2.2: graph of the function  $H$  (left) and stationary solution (right)

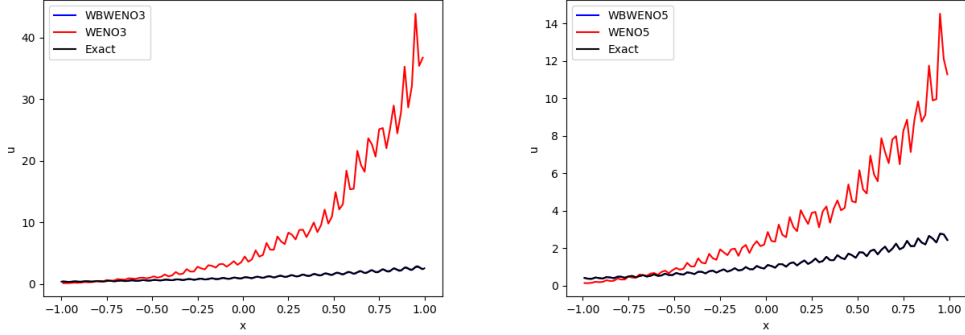


Figure 7: Test 5.2.2: exact solution and numerical solutions obtained at time  $t = 1$  and a mesh of 100 cells. Left: WBWENO3, WENO3. Right: WBWENO5, WENO5

Cells	WENO5		WBWENO5
	Error	Order	Error
20	7.7695E-07	-	2.2759e-16
40	3.5170E-09	7.78	1.5543e-16
80	2.0005E-10	4.13	1.1657e-16
160	1.0352E-11	4.27	2.9559e-16

Table 3: Test 5.2.1. Errors in  $L^1$  norm and convergence rates for WENO5 and WBWENO5 at time  $t = 8$ .

### 5.2.2 Preservation of a stationary solution with oscillatory smooth $H$

Let us consider now (32) with a function  $H$  that has an oscillatory behavior:

$$H(x) = x + 0.1 \sin(100x), \quad (34)$$

(see Figure 6). We consider again the interval  $[-1, 1]$  and we take as initial condition the stationary solution

$$u(x) = e^{x+0.1 \sin(100x)},$$

(see Figure 6) and, as boundary conditions, the value of this stationary solution is also imposed at the ghost cells.

We consider a 100-cell mesh, so that the period of the oscillations is close to  $\Delta x$ . Figure 7 shows the numerical solutions at time  $t = 1$  corresponding to WBWENO $p$ , WENO $p$ ,  $p = 3, 5$ : while the well-balanced methods preserve the stationary solution with machine precision, the non well-balanced methods give a wrong

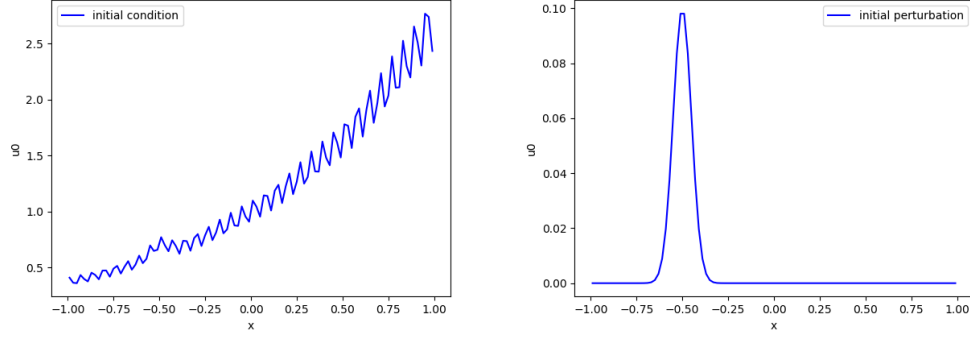


Figure 8: Test 5.2.3: initial condition. Left: graph. Right: difference with the stationary solution

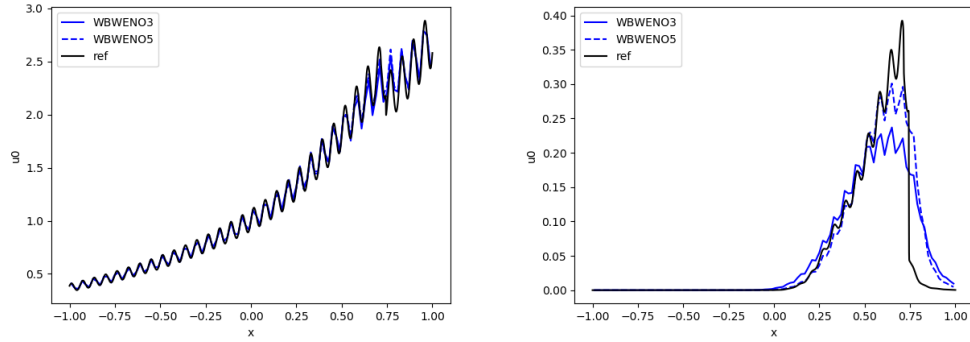


Figure 9: Test 5.2.3: reference and numerical solutions obtained with WBWENO3 and WBWENO5 at time  $t = 1$  and a mesh of 100 cells. Left: graphs. Right: difference with the stationary solutions

numerical solution. Of course, they give more accurate solutions if the mesh is refined: see next paragraph, where the reference solution is computed using WENO3.

### 5.2.3 Perturbation of a stationary solution with oscillatory smooth $H$

We consider again Burgers' equation (32) with  $H$  as in (34), and an initial condition that is the stationary solution approximated in the previous test with a small perturbation

$$u_0(x) = e^{x+0.1 \sin(100x)} + 0.1e^{-200(x+5)^2},$$

(see Figure 8). If a mesh with 100 cells is used, the non well-balanced methods are unable to follow the evolution of the perturbation, since the numerical errors observed in the previous test are much larger than the perturbation. Let us see what happens when well-balanced methods are used: Figure 9 shows the numerical solutions obtained with WBWENO3 and WBWENO5 and a reference solution computed with WENO3 using a mesh of 5000 cells at time  $t = 1$ . As it can be seen, both methods are able to follow the evolution of the perturbation.

### 5.2.4 Preservation of a stationary solution with piecewise continuous $H$

Let us consider now (32) with a piecewise continuous function  $H$ :

$$H(x) = \begin{cases} 0.1x & \text{if } x \leq 0; \\ 0.9 + x & \text{otherwise;} \end{cases} \quad (35)$$

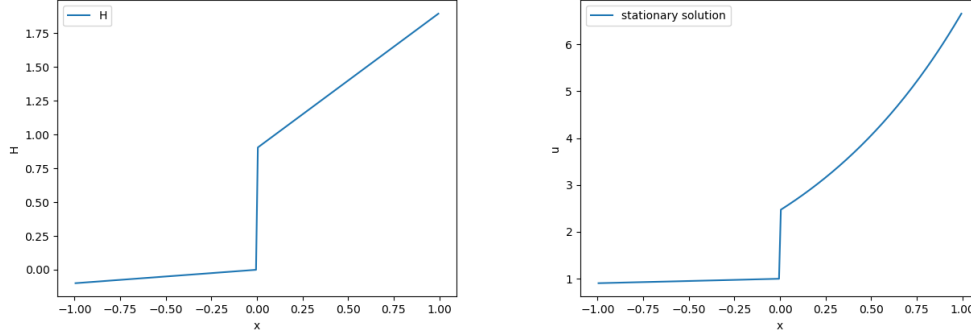


Figure 10: Test 5.2.4: graph of the function  $H$  (left) and stationary solution (right)

(see Figure 10). We consider again the interval  $[-1, 1]$  and we take as initial condition the stationary solution

$$u(x) = \begin{cases} e^{0.1x} & \text{if } x \leq 0; \\ e^{0.9+x} & \text{otherwise;} \end{cases} \quad (36)$$

(see Figure 10) and, as boundary conditions, the value of this stationary solution is also imposed at the ghost cells. WBWENO $p$ ,  $p = 3, 5$  preserve the stationary solution again with machine accuracy: see Table 4.

Cells	WBWENO3	WBWENO5
100	7.4984E-15	5.3790E-14
200	1.5432E-16	1.7763E-16
300	2.1464E-16	4.1611E-15

Table 4: Test 5.2.4. Errors in  $L^1$  norm for WBWENO3 and WBWENO5 at time  $t = 1$ .

For WENO methods, the non-conservative product appearing at the source term is discretized by (26) with two different definitions of  $s_{I-1/2}$ : a centered one

$$s_{I-1/2} = s(0.5(u_{I-1} + u_I)) \quad (37)$$

or an upwind one

$$s_{I-1/2} = \left( \frac{1 + \text{sign}(u_{I-1/2})}{2} \right) s(u_{I-1}) + \left( \frac{1 - \text{sign}(u_{I-1/2})}{2} \right) s(u_I). \quad (38)$$

Here,  $I - 1/2$  is the index of the intercell is located and  $u_{I-1/2}$  is the arithmetic mean of  $u_{I-1}$  and  $u_I$ .

In Figure 11 we compare the exact solution with the numerical solutions obtained at time  $t = 1$  obtained with WBWENO3 using a 300-cell mesh (its graph and the one of the exact solution are identical at the scale of the figure) and with WENO3 or WENO5 using different implementations:

- WENO3-UPW1: WENO3 with upwind implementation and (38);
- WENO3-UPW2: WENO3 with upwind implementation and (37);
- WENO3-LF: WENO3 with LF implementation and (38);
- WENO5-LF: WENO5 with LF implementation and (38).

As it can be observed, the results of the WENO methods depends on the chosen implementation, on the numerical definition of the source term, and on the order. Moreover, these differences remain as  $\Delta x$  tends to 0. This is in good agreement with the difficulties of convergence of finite difference methods to nonconservative systems: see [7].



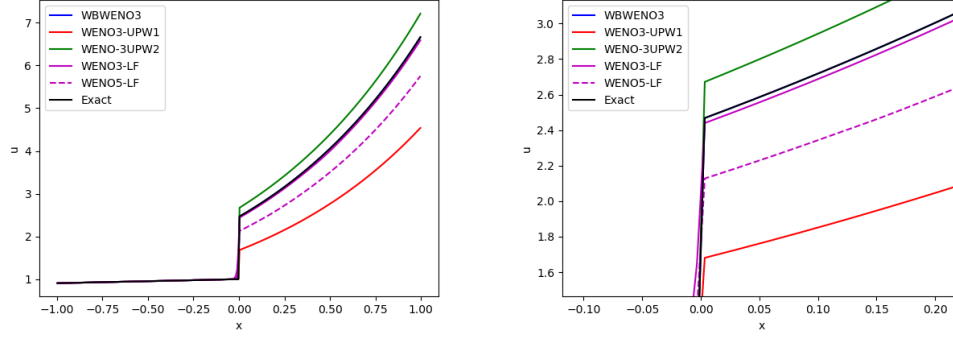


Figure 11: Test 5.2.3: exact and numerical solutions obtained at time  $t = 1$  with WBWENO3, WENO3-UPW1, WENO3-UPW2, WENO3-LF, WENO5-LF. Left: global view. Right: zoom close to the discontinuity

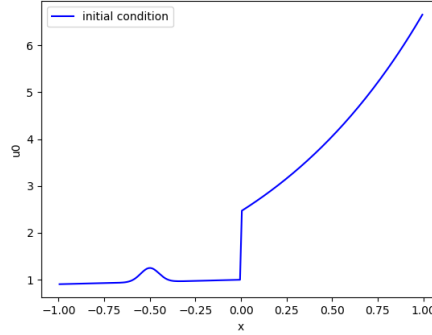


Figure 12: Test 5.2.5: initial condition.

### 5.2.5 Perturbation of a stationary solution with piecewise continuous $H$

We consider again (32) with (35) and an initial condition that is the stationary solution approximated in the previous test with a small perturbation

$$\tilde{u}_0(x) = u(x) + 0.3e^{-200(x+5)^2},$$

where  $u$  is given by (36): see Figure 12. Again, WENO $p$ ,  $p = 3, 5$  are unable to follow the evolution of the perturbation, since they are not able to preserve the stationary solution. Figure 12 shows the initial condition and the numerical solutions obtained with WBWENO $p$  and WB1WENO $p$ ,  $p = 3, 5$  with a mesh of 300 cells together with a reference solution computed with WBWENO3 using a mesh of 5000 cells at time  $t = 0.5$ . As it can be seen, while WB1WENO $p$  preserves the stationary solution (the results obtained in the previous test are indistinguishable from those obtained with WBWENO $p$ ), once the perturbations arrive to the discontinuity, the stationary solution is no longer preserved after its passage: see the discussion in Section 4.

## 5.3 Shallow water equations

We consider the shallow water system (1) with:

$$U = \begin{bmatrix} h \\ q \end{bmatrix}, \quad F(U) = \begin{bmatrix} q \\ \frac{q^2}{h} + \frac{g}{2}h^2 \end{bmatrix}, \quad S(U) = \begin{bmatrix} 0 \\ gh \end{bmatrix}. \quad (39)$$

The variable  $x$  makes reference to the axis of the channel and  $t$  is time;  $q(x, t)$  and  $h(x, t)$  represent the mass-flow and the thickness, respectively;  $g$ , the acceleration due to gravity;  $H(x)$ , the depth measured from a fixed level of reference;  $q(x, t) = h(x, t)u(x, t)$ , with  $u$  the depth averaged horizontal velocity.

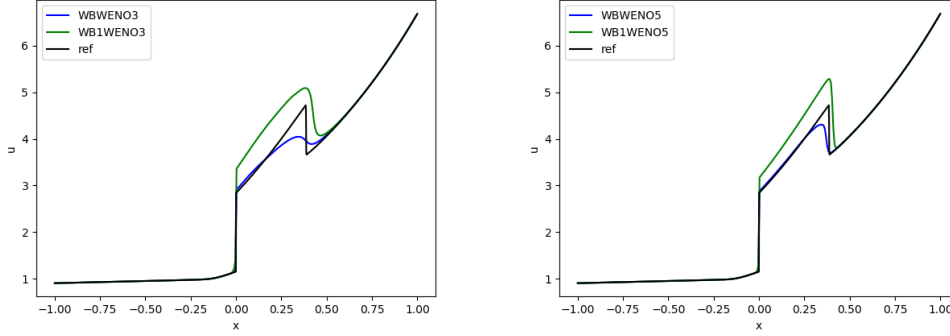


Figure 13: Test 5.2.5: numerical solutions obtained with WBWENOp and WB1WENOp at time  $t = 0.5$  and a mesh of 300 cells: left  $p = 3$ , right  $p = 5$

For this system (21) writes as follows:

$$\begin{cases} \frac{dq}{d\sigma} = 0, \\ \frac{d}{d\sigma} \left( \frac{q^2}{h} + \frac{g}{2} h^2 \right) = gh, \end{cases}$$

whose solutions are implicitly given by:

$$q = C_1, \quad \frac{1}{2} \frac{q^2}{h^2} + gh - g\sigma = C_2.$$

Therefore, the solution of (23) is implicitly given by

$$q_i^* = q_i, \quad \frac{1}{2} \frac{q_i^2}{h_i^{*2}} + gh_i^* - g\sigma = C_2.$$

with

$$C_2 = \frac{1}{2} \frac{q_i^2}{h_i^2} + gh_i - gH_i.$$

Therefore, at a point  $x_j$  of the stencil, one has  $q_i^*(H_j) = q_i$  and  $h_i^*(H_j)$  has to be a positive root of the polynomial:

$$P(h) = gh^3 - (C_2 + gH_j)h^2 + \frac{1}{2}q_i^2.$$

This polynomial can have two, one, or zero positive roots. In the first case, one of the roots corresponds to a supercritical state and the other one to a subcritical state: the root corresponding to the same regime of the state  $U_i$  is selected. In the third case, there is no equilibrium to be preserved, and (3) is used to update  $U_i$ . When  $U_i$  is critical two choices are possible, and a criterion is required.

Once  $h_i^*$  has been computed at the points of the stencil, the reconstruction procedure is applied to

$$\mathcal{F}_j = F(U_j) - F(U_i^*(x_j)) = \left[ \frac{q_i^2}{h_j} + \frac{g}{2} h_j^2 - \frac{q_i^2}{h_i^*(H_j)} - \frac{g}{2} (h_i^*(H_j))^2 \right], \quad j = i - r, \dots, i + s.$$

Water at rest equilibria are the 1-parameter family of stationary solutions corresponding to  $C_1 = 0$ :

$$q = 0, \quad h - H = \bar{\eta},$$

where  $\bar{\eta}$  is a constant. It is easy to obtain a family of numerical methods that only preserve this particular family, the reconstruction operator has to be applied to

$$F(U_j) = F(U_j) - \left[ \frac{0}{2} (h_i - H_i + H_j)^2 \right], \quad j = i - r, \dots, i + s.$$

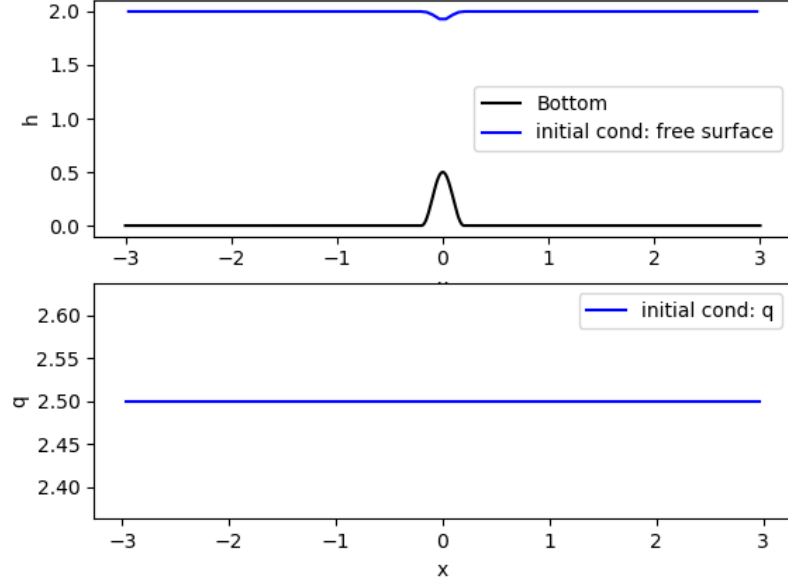


Figure 14: Test 5.3.1: initial condition: surface elevation (up) and mass-flow (down)

### 5.3.1 Preservation of a subcritical stationary solution

We consider the shallow water system with the bottom depth given by

$$H(x) = \begin{cases} -0.25(1 + \cos(5\pi x)) & \text{if } -0.2 \leq x \leq 0.2; \\ 0 & \text{otherwise;} \end{cases} \quad (40)$$

and we take as initial condition the subcritical stationary solution  $(h^*, q^*)$  characterized by

$$q^* = 2.5. \quad h^*(-3) = 2.$$

see Figure 14. Together with WENO $p$  and WBWENO $p$ , we also consider here WB1WENO $p$ : the numerical method that only preserves the stationary solution taken as initial condition. Table 5 shows the errors and order of convergence of the different methods. Figures 15 and 16 show the numerical results obtained with a 100-cell mesh using WENO $p$  and WBWENO $p$ ,  $p = 3, 5$  at time  $t = 4$ .

Cells	WB1WENO3	WBWENO3	WENO3		WB1WENO5	WBWENO5	WENO5	
	Error	Error	Error	Order	Error	Order	Error	Order
50	0	0	3.6778E-1	-	0	0	3.0347E-1	-
100	3.1974E-16	2.6645E-17	9.3955E-2	1.968	1.6546E-14	2.6645E-17	3.1542E-2	3.266
200	3.8635E-16	4.6629E-17	1.3430E-2	2.806	3.1974E-16	4.6629E-17	2.8092E-3	3.489
400	8.8862E-15	4.6629E-17	1.7931E-3	2.904	8.6410E-13	4.6629E-17	3.5654E-4	2.977

Table 5: Test 5.3.1. Errors in  $L^1$  norm and convergence rates for WB1WENO $p$ , WBWENO $p$  and WENO $p$ ,  $p = 3, 5$  at time  $t = 4$ .

### 5.3.2 Perturbation of a subcritical stationary solution

In this test case, we consider an initial condition which is obtained by adding a small perturbation to the stationary solution considered in the previous case. More precisely, a perturbation of size  $\Delta h = 0.02$  is added

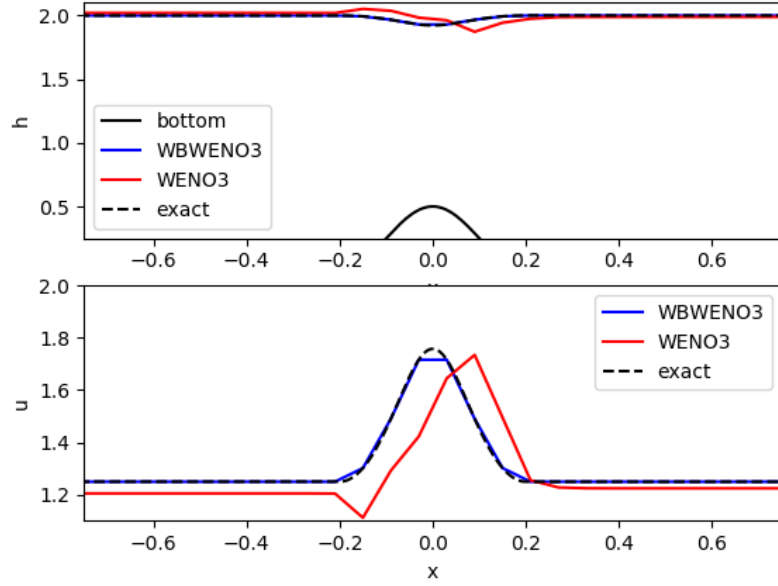


Figure 15: Test 5.3.1: Zoom of the numerical solutions obtained at time  $t = 4$ . with WBWENO3 and WENO3 using a mesh of 100 cells: surface elevation (up) and mass-flow (down)

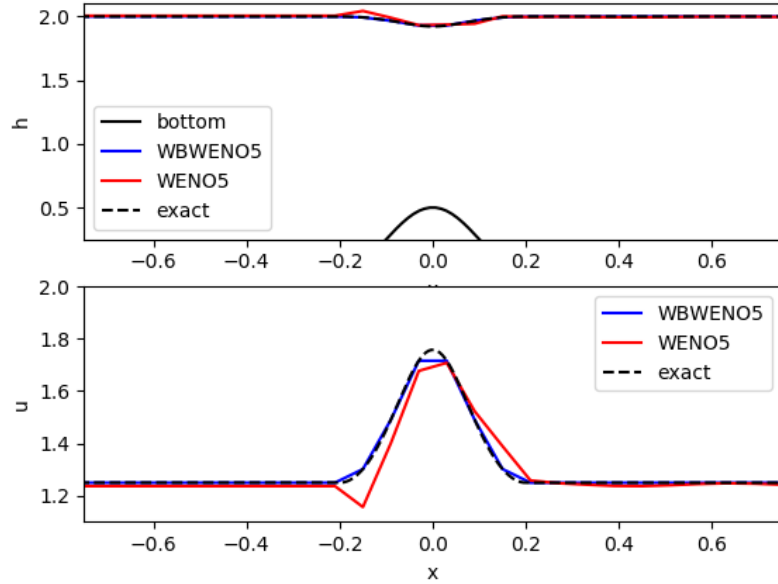


Figure 16: Test 5.3.1: Zoom of the numerical solutions obtained at time  $t = 4$ . with WBWENO5 and WENO5 using a mesh of 100 cells: surface elevation (up) and mass-flow (down).

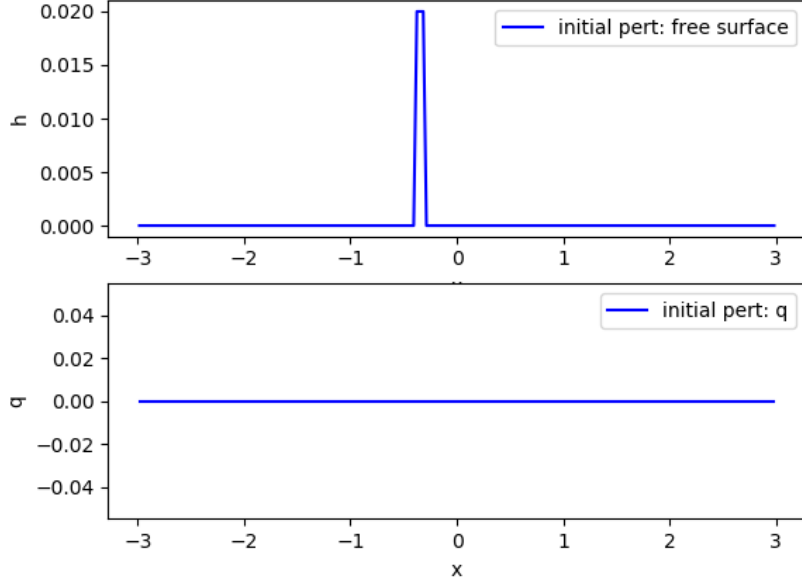


Figure 17: Test 5.3.2: initial perturbation: surface elevation (up) and mass-flow (down)

to the thickness  $h$  in the interval  $[-0.4, -0.3]$ : see Figure 17. Figures 18 and 19 show the difference between the numerical solutions obtained with WENO $p$ , WBWENO $p$ ,  $p = 3, 5$  and the stationary solution. A reference solution has been computed with WENO3 in a mesh of 2000 cells. Again, the solutions obtained with WBWENO $p$  and WB1WENO $p$ ,  $p = 3, 5$  are indistinguishable.

### 5.3.3 Preservation of a transcritical stationary solution over a discontinuous bottom

We consider now a discontinuous topography given by the depth function

$$H = \begin{cases} -0.25(1 + \cos(5\pi(x + 1.2))) & \text{if } -1.4 \leq x \leq -1, \\ 1 & \text{if } x > 0, \\ 0 & \text{otherwise.} \end{cases} \quad (41)$$

Although the application of the shallow water model for the simulation of a flow over a discontinuous bottom can be debatable, many authors have used it to obtain a rough simulation of the flow behavior. In any case, we consider here this application as a challenging test from the numerical analysis point of view: once the admissible jumps at a discontinuity of  $H$  have been chosen, the challenge is to design numerical methods that preserve the admissible stationary solutions. According to the discussion in Section 4, a pair of states  $U^\pm = [h^\pm, q^\pm]^T$  constitute an admissible jump of a weak solution at  $x = 0$  (the discontinuity point of  $H$ ) if the following equalities are satisfied:

$$q^+ = q^-, \quad \frac{1}{2} \frac{(q^+)^2}{(h^+)^2} + gh^+ - gH^+ = \frac{1}{2} \frac{(q^-)^2}{(h^-)^2} + gh^- - gH^-,$$

where  $H^- = 0$ ,  $H^+ = 1$ .

For WENO and WB1WENO methods, the equations for the neighbor nodes of the discontinuity  $x_{I-1/2}$  are given by (26) and (27) respectively, with

$$S_{I-1/2} = S(0.5(U_I + U_{I-1})). \quad (42)$$

We take now as initial condition the transcritical admissible stationary solution characterized by:

$$q^* = 2.5, \quad h^*(0) = \frac{(2.5)^{2/3}}{g^{1/3}}$$

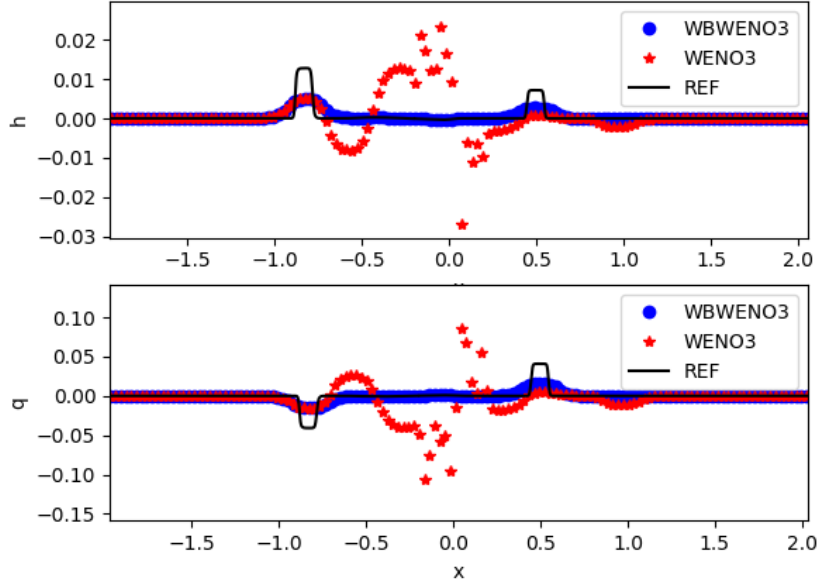


Figure 18: Test 5.3.2: Zoom of the differences between the numerical solutions obtained at time  $t = 0.15$  with WBWENO3, and WENO3 using a mesh of 200 cells and the stationary solution: surface elevation (up) and mass-flow (down)

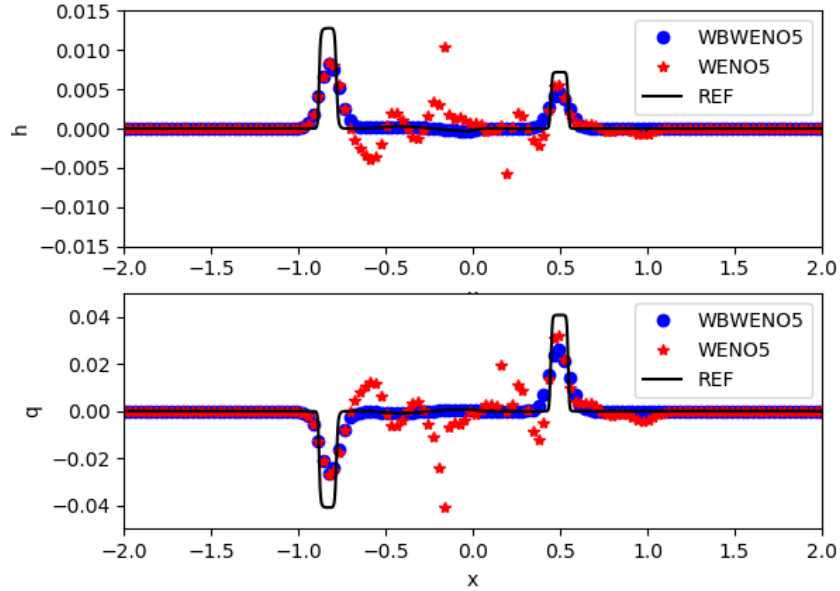


Figure 19: Test 5.3.2: Zoom of the differences between the numerical solutions obtained at time  $t = 0.15$  with WBWENO5, and WENO5 using a mesh of 200 cells and the stationary solution: surface elevation (up) and mass-flow (down)

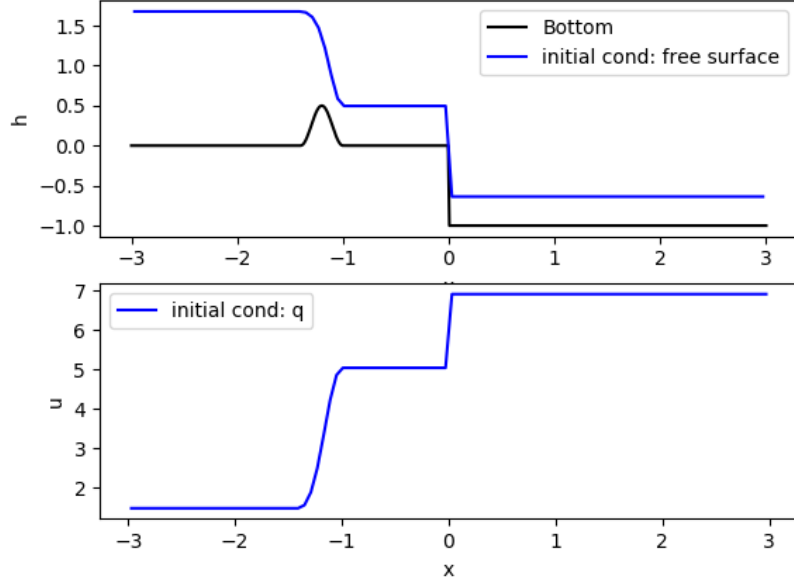


Figure 20: Test 5.3.3: initial condition: surface elevation (up) and velocity (down)

that is subcritical at the left of  $x = 0$  and supercritical at its right: see Figure 20.

Figures 21 and 22 show the results obtained with  $WENO_p$  and  $WBWENO_p$ ,  $p = 3, 5$  using a mesh of 100 cells at time  $t = 4$ . Table 6 shows the error in  $L^1$  norm: according to the discussion in Section 4,  $WBWENO_p$  and  $WB1WENO_p$  preserve the stationary solution to machine precision, while the solutions provided by  $WENO_p$  are not close to the stationary solution.

WB1WENO3	WBWENO3	WENO3	WB1WENO5	WBWENO5	WENO5
7.9602E-16	7.9602E-16	1.3178	7.9602E-16	7.9602E-16	0.6229

Table 6: Test 5.3.3. Errors in  $L^1$  norm for  $WB1WENO_p$ ,  $WBWENO_p$  and  $WENO_p$ ,  $p = 3, 5$  at time  $t = 4$ .

#### 5.3.4 Perturbation of a transcritical stationary solution over a discontinuous bottom

We consider now an initial condition which is obtained by adding a small perturbation to the stationary solution considered in the previous one. More precisely, a perturbation of size  $\Delta h = 0.02$  is added to the thickness  $h$  in the interval  $[-0.4, -0.3]$ : see Figure 17. Figures 23 and 24 show the difference between the numerical solutions obtained with  $WENO_p$ ,  $WBWENO_p$ ,  $WB1WENO_p$ ,  $p = 3, 5$  and the stationary solution. A reference solution has been computed with  $WBWENO3$  in a mesh of 2000 cells. According to the discussion in Section 4,  $WB1WENO_p$  can deviate from the stationary solution once the perturbation reaches the discontinuity of  $H$ . Nevertheless, the differences in this case with  $WBWENO_p$  are relatively small: see Figure 23 (right) and 24 (right). The numerical treatment of the source term seems to add some more numerical diffusion; this can be observed clearly for  $p = 5$ .

#### 5.3.5 Mass conservation and computational cost

In order to measure the mass conservation properties of the different methods and compare the computational cost, we consider now the depth function

$$H(x) = \begin{cases} 0.13 + 0.05(x - 10)^2 & \text{if } 8 \leq x \leq 12; \\ 0.33 & \text{otherwise.} \end{cases}$$

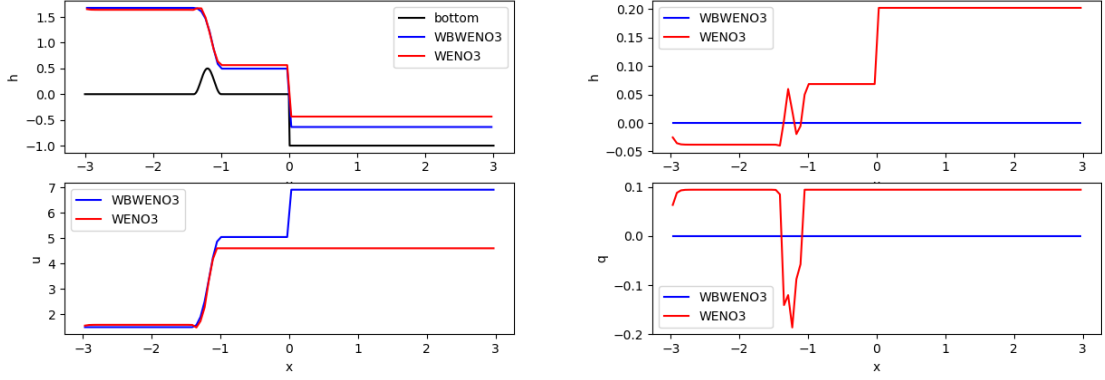


Figure 21: Test 5.3.3. Left: Numerical solutions obtained at time  $t = 4$ . with WBWENO3, and WENO3 using a mesh of 100 cells: surface elevation (up) and velocity (down). Right: Difference between the numerical solutions and the stationary solution: surface elevation (up) and mass-flow (down)

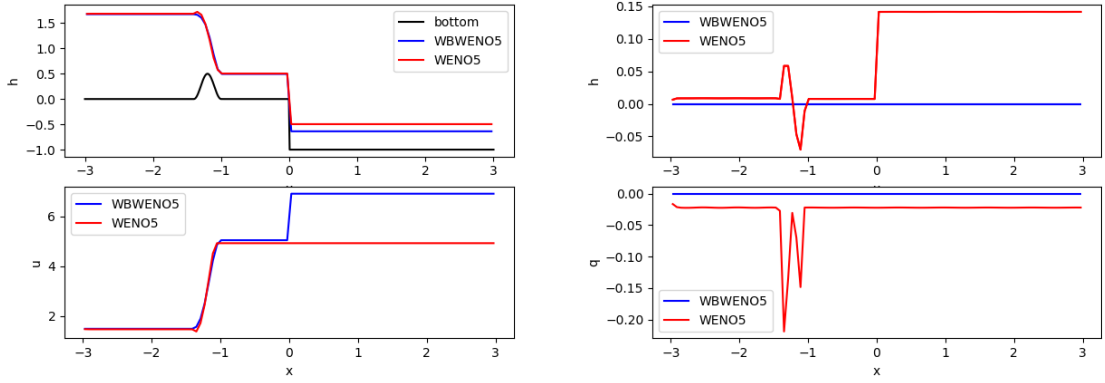


Figure 22: Test 5.3.3. Left: Numerical solutions obtained at time  $t = 4$ . with WBWENO5, and WENO5 using a mesh of 100 cells: surface elevation (up) and velocity (down). Right: Difference between the numerical solutions and the stationary solution: surface elevation (up) and mass-flow (down)

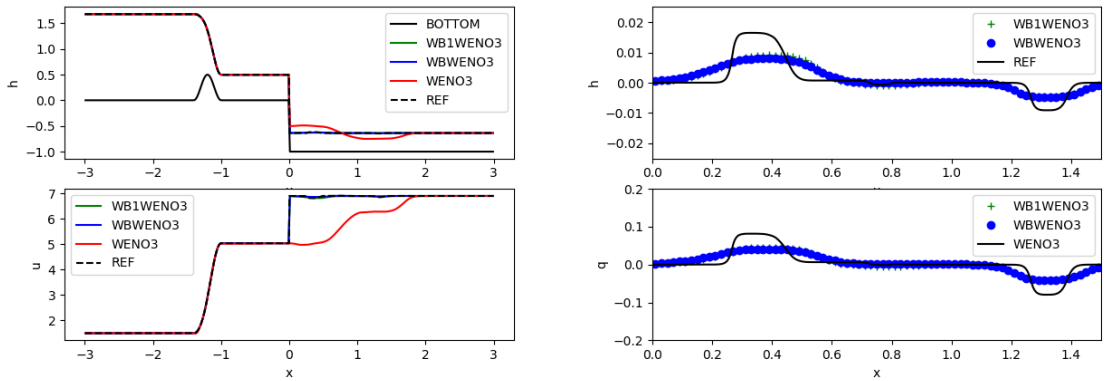


Figure 23: Test 5.3.4. Left: Numerical solutions obtained at time  $t = 0.2$  with WB1WENO3, WBWENO3, and WENO3 using a mesh of 300 cells: surface elevation (up) and velocity (down). Right: Difference between the numerical solutions obtained with WB1WENO3 and WBWENO3 and the stationary solution: surface elevation (up) and mass-flow (down)



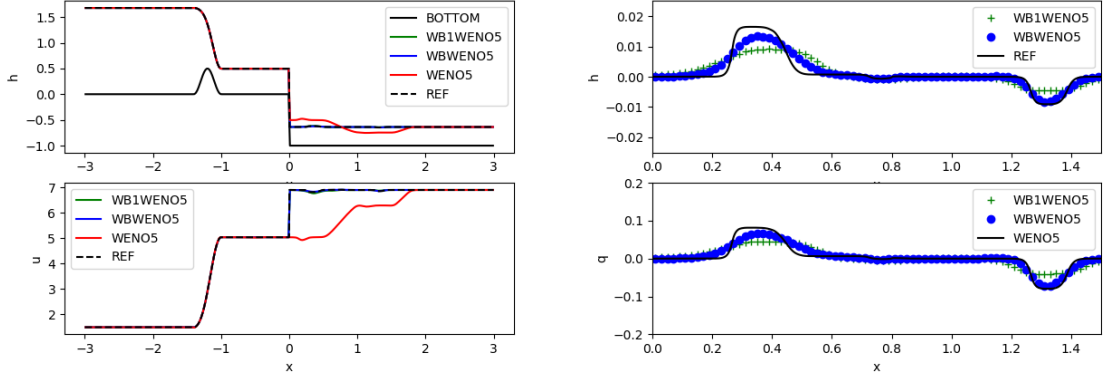


Figure 24: Test 5.3.4. Left: Numerical solutions obtained at time  $t = 0.2$  with WB1WENO5, WBWENO5, and WENO5 using a mesh of 300 cells: surface elevation (up) and velocity (down). Right: Difference between the numerical solutions obtained with WB1WENO5 and WBWENO5 and the stationary solution: surface elevation (up) and mass-flow (down)

and the initial condition

$$h_0(x) = h^*(x) + 0.5\chi_{[5,7]}, \quad q_0(x) = 1,$$

where  $h^*(x)$  is the thickness corresponding to the stationary solution characterized by

$$q^* = 1, \quad h^*(10) = 1,$$

and  $\chi_{[a,b]}$  denotes the characteristic function of an interval  $[a, b]$ : see Figure 25. The computational domain is the interval  $[-10, 30]$  and the boundary conditions are  $h = h^*$ ,  $q = 1$  at both extremes. The simulation is run until time  $t = 0.5$ . Figure 26 shows a zoom of the results obtained with WENO3, WBWENO3, WB1WENO3 at time  $t = 0.5$  using a mesh of 200 cells. The conclusions are the same as in the previous test case.

The total mass water at time  $t^n$  is computed by

$$m_n = \Delta x \sum_i h_i^n.$$

Since the boundary conditions are equal at both extremes of the interval and the simulation is stopped before the waves arrive at the boundaries, the total mass is expected to be preserved. Table 7 shows the maximum relative deviation of the total mass with respect to its initial value for the different numerical methods, i.e.

$$\max_n \left| \frac{m_n - m_0}{m_0} \right|$$

WB1WENO3	WBWENO3	WENO3	WB1WENO5	WBWENO5	WENO5
6.3454E-16	2.4969E-06	7.9318E-16	6.3454E-16	2.5714E-06	7.9318E-16

Table 7: Test 5.3.5.

According to the discussion in Section 3.4, WBWENO $p$ ,  $p = 3, 5$  do not preserve the total mass. Figure 27 shows the variation with time of these deviations for WBWENO3 and WBWENO5.

Finally, we compare the computational cost of the different numerical methods in this test case: Table 8 compares the averaged CPU times of 10 runs using WBWENO $p$ , WB1WENO $p$  and WENO $p$ ,  $p = 3, 5$ . Each row of the table shows the averaged CPU time corresponding to WBWENO $p$  and WB1WENO $p$  divided by the one corresponding to WENO $p$ . Figure 28 shows the graph of the CPU time as a function of  $\log_2(N)$ . As can be seen, the use of the well-balanced technique that allows one to capture every stationary solution increases the CPU time between 2 and 3.75 times, while the ratios corresponding to the one that preserves only one particular stationary solution go from 1.1 to 2.1.

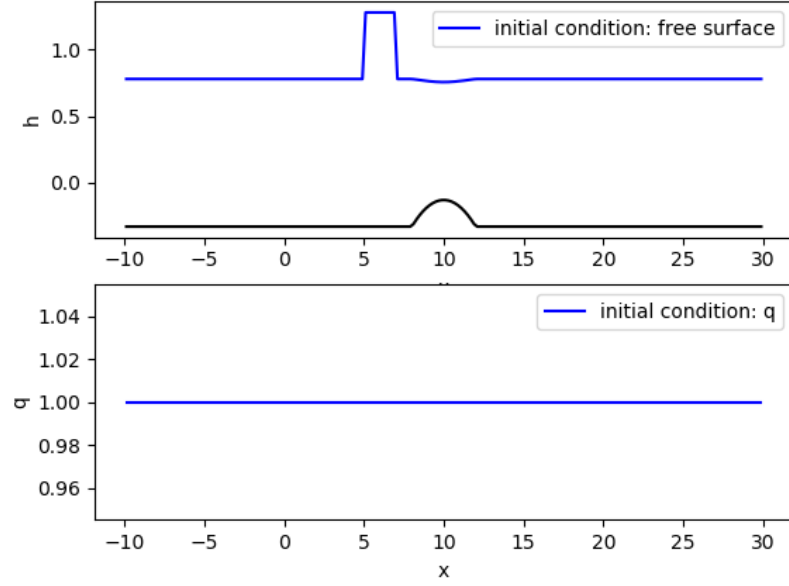


Figure 25: Test 5.3.5: initial condition: surface elevation (up) and mass-flow (down)

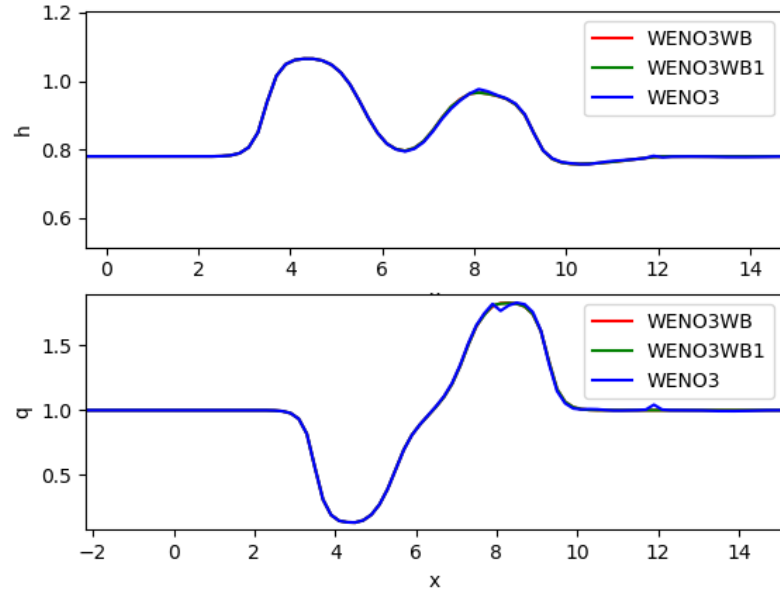


Figure 26: Test 5.3.5: Zoom of the numerical solutions obtained at time  $t = 0.5$  with WB1WENO3, WBWENO3, and WENO3 using a mesh of 200 cells: surface elevation (up) and mass-flow (down)

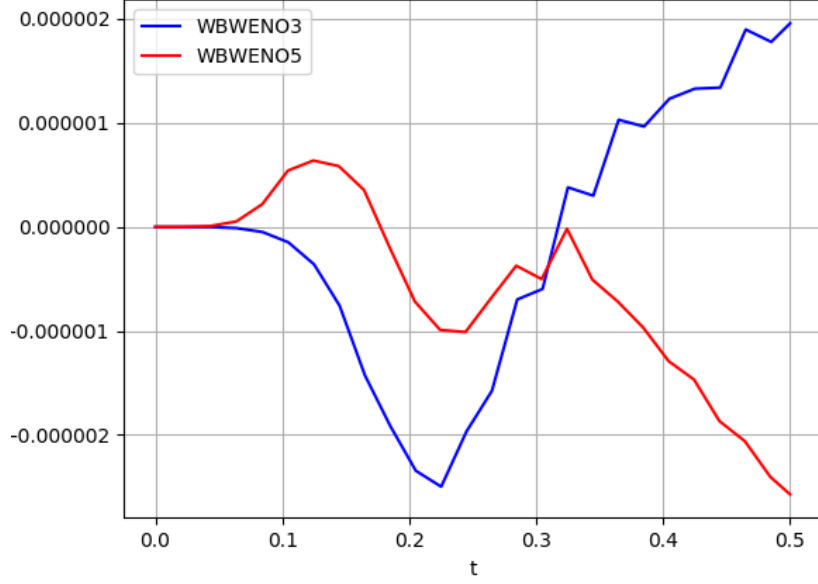


Figure 27: Test 5.3.5: Evolution of the relative deviation of the total mass with time for WBWENO3 and WBWENO5

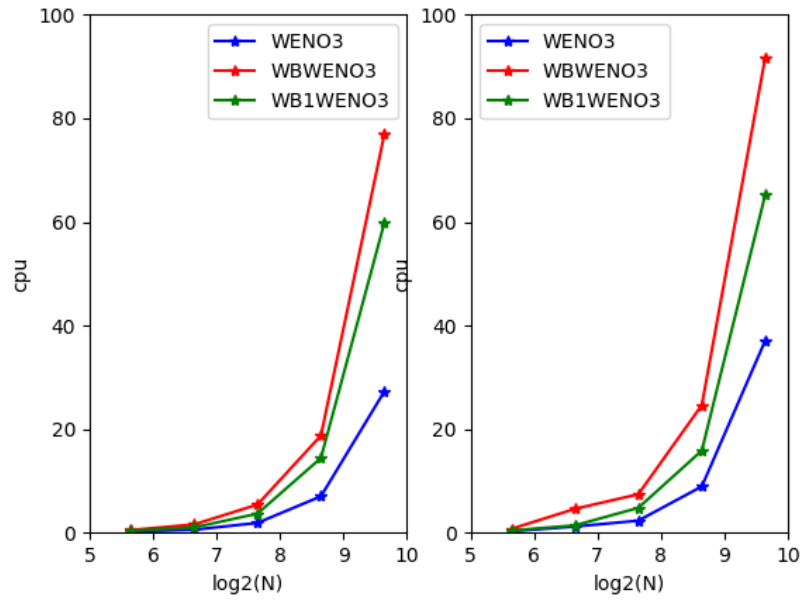


Figure 28: Test 5.3.5: cpu times as a function of  $\log_2(N)$  for WENO $p$ , WBWENO $p$  and WB1WENO $p$ ,  $p = 3, 5$

Cells	WBWENO3	WB1WENO3	WBWENO5	WB1WENO5
50	2.0353448	1.44154196	2.41255001	1.40896775
100	2.62843037	1.72058152	3.74834895	1.17608303
200	2.82185883	1.91835005	3.1523362	2.04117458
400	2.65968638	2.04649931	2.74958714	1.77160907
800	2.8173806	2.19114322	2.4709661	1.75789315

Table 8: Test 5.3.5. cpu times corresponding to WBWENO $p$  and WB1WENO $p$  divided by the one corresponding to WENO $p$  using meshes of  $N = 50, 100, 200, 400$  and  $800$  cells.

## 6 Conclusions

Two families of well-balanced high-order finite difference numerical methods have been introduced: one of them preserves every stationary solution while the second preserves only one particular stationary solution. The accuracy and the well-balanced properties of the methods have been analyzed. The methods have been applied to a number of numerical tests related to the linear transport equation with linear source term, Burgers' equation with nonlinear source terms, and the shallow water equations. A challenging test in which a transcritical solution of the shallow water over a discontinuous bottom is perturbed has been considered. The following conclusions can be drawn:

- For test cases in which there is only one known stationary solution involved, both families give essentially the same results when  $H$  is continuous.
- When  $H$  has discontinuities, both families preserve admissible discontinuous stationary solutions, but the methods that only preserve one stationary solution may fail when this solution is perturbed.
- When the system contains conservation laws, the numerical methods that only preserve one stationary solution are conservative for them which is not the case for the methods that preserve every stationary solution. The design of high-order finite difference WENO methods that have both properties (if it is possible) remains a challenge.
- The numerical methods that only preserve one stationary solution are computationally less expensive.

The main difficulty in applying the methods introduced here to arbitrary systems of balance laws is related to the numerical resolution of a Cauchy problem whose ODE system is not in normal form. Further extensions would include the application to general systems by solving numerically the Cauchy problems.

The strategy introduced here to design numerical methods that preserve only one known stationary solution can be easily extended to multidimensional problems. Nevertheless, the design of well-balanced methods that preserve general stationary solutions for multidimensional problems remains a major challenge. We hope that the application of numerical methods for solving the Cauchy problems for general 1d problems will give some hints to tackle this challenge, although the boundary value problems to be solved will be related to nonlinear PDEs in that case.

## References

- [1] J. P. Berberich, P. Chandrashekar, C. Klingenberg. High order well-balanced finite volume methods for multi-dimensional systems of hyperbolic balance laws. arXiv:1903.05154 (2019)
- [2] A. Bermúdez and M. E. Vázquez. Upwind methods for hyperbolic conservation laws with source terms. *Computers & Fluids*, 23(8):1049–1071 (1994).
- [3] A. Canestrelli, A. Siviglia, M. Dumbser, E. F. Toro. Well-balanced high-order centred schemes for non-conservative hyperbolic systems. Applications to shallow water equations with fixed and mobile bed. *Advances in Water Resources*, 32(6): 834–844 (2009).
- [4] V. Caselles, R. Donat, G. Haro. Flux-gradient and source-term balancing for certain high resolution shock-capturing schemes. *Computers & Fluids*, 38:16–36 (2009).

- [5] M. J. Castro, J.M. Gallardo J. López, and C. Parés. Well-balanced high order extensions of Godunov method for linear balance laws. *SIAM Journal on Numerical Analysis*, 46:1012–1039 (2008)
- [6] M. J. Castro, I. Gómez-Bueno, C. Parés. High-order well-balanced methods for systems of balance laws: a control-based approach. Submitted (2020).
- [7] M. J. Castro, P.G. LeFloch, M.L. Muñoz-Ruiz, C. Parés. Why many theories of shock waves are necessary: Convergence error in formally path-consistent schemes. *Journal of Computational Physics*, 227: 8107–8129, (2008).
- [8] M. J. Castro, J. A. López-García, and C. Parés. High order exactly well-balanced numerical methods for shallow water systems. *Journal of Computational Physics*, 246:242–264 (2013).
- [9] M. J. Castro, T. Morales, C. Parés. Well-balanced schemes and path-conservative numerical methods. *Hand book of Numerical Analysis*, 18: 131 – 175 (2017).
- [10] M. J. Castro, S. Ortega, C. Parés. Well-balanced methods for the shallow water equations in spherical coordinates *Computers & Fluids*, 157: 196–207 (2017).
- [11] Well-balanced high-order finite volume methods for systems of balance laws *Journal of Scientific Computing* to appear.
- [12] P. Chandrashekar and C. Klingenberg. A second order well-balanced finite volume scheme for Euler equations with gravity. *SIAM J. Sci. Comput.*, 37(3):B382–B402 (2015).
- [13] P. Chandrashekar and M. Zenk. Well-balanced nodal discontinuous Galerkin method for Euler equations with gravity. *J. Sci. Comput.*, 71(3):1062–1093 (2017).
- [14] A. Chertock, S. Cui, A. Kurganov, S.Özcan, and E. Tadmor. Well-balanced schemes for the Euler equations with gravitation: Conservative formulation using global fluxes. *J. Comput. Phys.*, 358:36–52 (2018).
- [15] G. Dal Maso, P. G. Lefloch, and F. Murat. Definition and weak stability of nonconservative products. *Journal de Mathématiques Pures et Appliquées*, 74(6):483–548 (1995).
- [16] R. Donat, A. Martínez-Gavara. Hybrid Second Order Schemes for Scalar Balance Laws *Journal of Scientific Computing volume* 48: 52–69(2011)
- [17] E. Gaburro, M. Dumbser, M. J. Castro. Direct Arbitrary-Lagrangian-Eulerian finite volume schemes on moving nonconforming unstructured meshes. *Computers & Fluids*, 159: 254–275 (2017).
- [18] E. Gaburro, M. J. Castro, M. Dumbser. Well-balanced Arbitrary-Lagrangian-Eulerian finite volume schemes on moving nonconforming meshes for the Euler equations of gas dynamics with gravity. *Monthly Notices of the Royal Astronomical Society*, 477(2): 2251– 2275 (2018).
- [19] E. Gaburro, M. J. Castro, M. Dumbser. A well balanced diffuse interface method for complex nonhydrostatic free surface flows, *Computers & Fluids*, 175: 180–198 (2018).
- [20] L. Gascón, J.M. Corberán. Construction of second-order TVD schemes for nonhomogeneous hyperbolic conservation laws. *Journal of Computational Physics* 172: 261–297 (2001)
- [21] S. Gottlieb and C.-W. Shu. Total variation diminishing Runge-Kutta schemes. *Mathematics of Computation of the American Mathematical Society*, 67(221): 73–85 (1998).
- [22] L. Grosheintz-Laval, R. Käppeli, High-order well-balanced finite volume schemes for the Euler equations with gravitation. *Journal of Computational Physics*, 378: 324–343 (2019).
- [23] G. Jiang, C.W.-Shu. Efficient implementation of weighted ENO schemes. *Journal of Computationalas Phycs*, 126: 202–228, 1996.
- [24] R. Käppeli and S. Mishra. Well-balanced schemes for the Euler equations with gravitation. *J. Comput. Phys.*, 259:199–219 (2014).

- [25] C. Klingenberg, G. Puppo and M. Semplice. Arbitrary order finite volume well-balanced schemes for the Euler equations with gravity. <https://arxiv.org/abs/1807.02341> (2018).
- [26] G. Li and Y. Xing. High order finite volume WENO schemes for the Euler equations under gravitational fields. *J. Comput. Phys.*, 316:145–163 (2016).
- [27] G. Li and Y. Xing. Well-balanced discontinuous Galerkin methods with hydrostatic reconstruction for the Euler equations with gravitation. *J. Comput. Phys.*, 352:445–462 (2018).
- [28] M. Lukáčová-Medvid’ová, S. Noelle, and M. Kraft. Well-balanced finite volume evolution Galerkin methods for the shallow water equations. *Journal of Computational Physics*, 221(1):122–147, (2007).
- [29] L. O. Müller, C. Parés, and E. F. Toro. Well-balanced High-order Numerical Schemes for One-dimensional Blood Flow in Vessels with Varying Mechanical Properties. *Journal of Computational Physics*, 242:53–85, (2013).
- [30] S. Noelle, N. Pankratz, G. Puppo, and J. R. Natvig. Well-balanced finite volume schemes of arbitrary order of accuracy for shallow water flows. *Journal of Computational Physics*, 213(2):474–499 (2006).
- [31] S. Noelle, Y. Xing, and C.-W. Shu. High-order well-balanced finite volume WENO schemes for shallow water equation with moving water. *Journal of Computational Physics*, 226(1):29–58 (2007).
- [32] C. Parés. Numerical methods for nonconservative hyperbolic systems: a theoretical framework. *SIAM Journal on Numerical Analysis*, 44:300–321 (2006).
- [33] C. Parés, M.L. Muñoz. On some difficulties of the numerical approximation of nonconservative hyperbolic systems. *SEMA Journal*, 23–52 (2009).
- [34] G. Russo and A. Khe. High order well balanced schemes for systems of balance laws. In *Hyperbolic problems: theory, numerics and applications*, volume 67 of *Proc. Sympos. Appl. Math.*, pages 919–928. Amer. Math. Soc., Providence, RI (2009).
- [35] C.-W. Shu., S. Osher. Efficient implementation of essentially non-oscillatory shock-capturing schemes. *Journal of Computational Physics*. 77: 439–471 (1988).
- [36] C.-W. Shu. Essentially non-oscillatory and weighted essentially non-oscillatory schemes for hyperbolic conservation laws. In Cockburn, B., Johnson, C., Shu, C.-W., Tadmor, E., and Quarteroni, A. (eds.), *Advanced Numerical Approximation of Nonlinear Hyperbolic Equations*, Lecture Notes in Mathematics, Vol. 1697, Springer, Berlin, pp. 325–432, 1998.
- [37] A. Thomann, M. Zenk, and C. Klingenberg. A second order positivity preserving well-balanced finite volume scheme for Euler equations with gravity for arbitrary hydrostatic equilibria. *International Journal for numerical methods in fluids*. 89(11): 465–482 (2019).
- [38] D. Varma and P. Chandrashekar. A second order well-balanced finite volume scheme for Euler equations with gravity. *Computers & Fluids*, 181: 292–313 (2019)
- [39] Y. Xing and C.W.-Shu. High-Order well-balanced finite difference WENO schemes with the exact conservation property for the shallow water equations. *Journal of Computational Physics*, 208: 206–227 (2006)
- [40] Y. Xing and C.W.-Shu. High-Order well-balanced finite difference WENO schemes for a class of hyperbolic systems with source terms. *Journal of Scientific Computing*, 27: 477–494 (2006)
- [41] Y. Xing and C.-W. Shu. High order well-balanced finite volume WENO schemes and discontinuous Galerkin methods for a class of hyperbolic systems with source terms. *Journal of Computational Physics*, 214(2):567–598 (2006).
- [42] Y. Xing and C.-W. Shu. High order well-balanced WENO scheme for the gas dynamics equations under gravitational fields. *J. Sci. Comput.*, 54(2-3):645–662 (2013).